

Suppressing proteasome mediated processing of topoisomerase II DNA-protein complexes preserves genome integrity

Nicholas Sciascia^{1,2}, Wei Wu^{1†}, Dali Zong^{1†}, Yilun Sun³, Nancy Wong¹, Sam John¹, Darawalee Wangsa⁴, Thomas Ried⁴, Samuel F Bunting⁵, Yves Pommier³, André Nussenzweig^{1*}

¹Laboratory of Genome Integrity, National Institutes of Health, Bethesda, United States; ²Institute for Biomedical Sciences, George Washington University, Washington, United States; ³Developmental Therapeutics Branch, National Institutes of Health, Bethesda, United States; ⁴Genetics Branch National Cancer Institute, National Institutes of Health, Bethesda, United States; ⁵Department of Molecular Biology and Biochemistry, Rutgers University, Piscataway, United States

Abstract Topoisomerase II (TOP2) relieves topological stress in DNA by introducing double-strand breaks (DSBs) via a transient, covalently linked TOP2 DNA-protein intermediate, termed TOP2 cleavage complex (TOP2cc). TOP2ccs are normally rapidly reversible, but can be stabilized by TOP2 poisons, such as the chemotherapeutic agent etoposide (ETO). TOP2 poisons have shown significant variability in their therapeutic effectiveness across different cancers for reasons that remain to be determined. One potential explanation for the differential cellular response to these drugs is in the manner by which cells process TOP2ccs. Cells are thought to remove TOP2ccs primarily by proteolytic degradation followed by DNA DSB repair. Here, we show that proteasome-mediated repair of TOP2cc is highly error-prone. Pre-treating primary splenic mouse B-cells with proteasome inhibitors prevented the proteolytic processing of trapped TOP2ccs, suppressed the DNA damage response (DDR) and completely protected cells from ETO-induced genome instability, thereby preserving cellular viability. When degradation of TOP2cc was suppressed, the TOP2 enzyme uncoupled itself from the DNA following ETO washout, in an error-free manner. This suggests a potential mechanism of developing resistance to topoisomerase poisons by ensuring rapid TOP2cc reversal.

***For correspondence:**

andre_nussenzweig@nih.gov

†These authors contributed equally to this work

Competing interests: The authors declare that no competing interests exist.

Funding: See page 23

Received: 08 November 2019

Accepted: 12 February 2020

Published: 14 February 2020

Reviewing editor: Maureen Murphy, The Wistar Institute, United States

© This is an open-access article, free of all copyright, and may be freely reproduced, distributed, transmitted, modified, built upon, or otherwise used by anyone for any lawful purpose. The work is made available under the [Creative Commons CC0 public domain dedication](https://creativecommons.org/licenses/by/4.0/).

Introduction

Topoisomerase II (TOP2) is an evolutionarily conserved enzyme capable of generating reversible double strand breaks (DSBs) in DNA, which enables the resolution of problematic DNA topological structures that arise during normal cellular processes, such as transcription, replication, and mitosis. This process is mediated by the topoisomerase II cleavage complex (TOP2cc), a transient DNA-protein complex that is formed when each monomer of the dimeric TOP2 anchors itself to the DNA backbone via a covalent 5'-phosphotyrosyl bond. A second DNA strand can then be passed through the enzyme-bridged DSB, after which the break is re-ligated. Under physiological conditions, topoisomerases reliably execute this reaction without error, as TOP2ccs are highly reversible and short lived (Pommier *et al.*, 2016). However, when they become trapped, the abortive TOP2ccs fail to re-ligate the transient DSB intermediate, presenting a severe threat to genome integrity which must be

eLife digest Molecules of DNA contain the archive of a cell's genetic information and identity. DNA comprises two strands that twist together into a structure known as a double helix. Physical tension tends to build up in the double helix that can cause it to break apart. To avoid this, cells have an enzyme called Topoisomerase II (TOP2) that relieves the tension by attaching itself to DNA and breaking it in a controlled way before re-sealing the break.

Drugs known as TOP2 poisons stop TOP2 from working and trap it on the DNA, which may lead to cells accumulating DNA breaks and eventually dying. Cancer cells are particularly prone to acquiring breaks in their DNA, and TOP2 poisons are therefore often used as part of chemotherapy treatments for cancer. However, it remains unclear why TOP2 poisons are more effective at killing some types of cancer cells than others.

It is thought that a molecular machine, known as the proteasome, helps cells repair the damage caused by TOP2 poisons by removing the trapped TOP2 proteins and allowing DNA repair proteins access to the broken DNA underneath. Now, Sciascia et al. have used a genetic approach to study the relationship between the proteasome and DNA repair in mouse cells exposed to TOP2 poisons.

The experiments found that when the proteasome removed TOP2 proteins that had become trapped on DNA, the subsequent DNA repair was prone to errors. Pre-treating mouse cells with another drug that inhibited the proteasome protected the cells from the effects of the TOP2 poison. Once the TOP2 poison had left the cells, the previously trapped TOP2 proteins correctly fixed the DNA and detached as they would normally. As a result, cells that had been treated with a proteasome inhibitor were more likely to survive treatment with TOP2 poisons.

Since both TOP2 poisons and proteasome inhibitors are clinically approved drugs for treating cancer they can be, and already have been, tested for use together in combination drug therapies. However, these findings suggest that caution should be taken when using these drugs together, because instead of harming the cancer cells, the proteasome inhibitors may protect the cells from the toxic effects of TOP2 poisons.

resolved quickly via the DNA repair machinery. The resolution of TOP2ccs is, therefore, crucial for cell survival.

TOP2 poisons, such as the anti-cancer agent etoposide (ETO), efficiently trap and stabilize TOP2ccs (*Muslimović et al., 2009; Nitiss, 2009a; Pommier et al., 2016*). The accumulation of these TOP2 DNA-protein complexes can create significant problems for cells by stalling replication forks and the transcription apparatus, generating torsional and genotoxic stress, which leads to the accumulation of single and double strand DNA breaks (*Cowell and Austin, 2012; Muslimović et al., 2009*). How these abortive TOP2ccs are recognized and targeted by the DNA damage response (DDR) remains unclear.

It has been suggested that a robust DNA damage response (DDR) is elicited only after ETO-trapped TOP2ccs have been converted to 'clean' protein-free DSB ends (*Mårtensson et al., 2003; Sunter et al., 2010; Zhang et al., 2006*). This suggests that a DSB shielded by a covalently bound protein can evade detection. Several mechanisms exist for removal of trapped TOP2ccs. However, the factors that determine how a cell chooses to deploy them are complex and remain poorly understood. The covalently-linked TOP2 protein is partially or completely degraded by the 26S proteasome, after which the residual DNA-peptide adduct is hydrolyzed by tyrosyl-DNA phosphodiesterase 2 (TDP2) to release the remnants of the entrapped protein (*Ledesma et al., 2009; Gómez-Herreros et al., 2013; Lee et al., 2018; Sunter et al., 2010; Zagnoli-Vieiral and Caldecott, 2017*). Current evidence suggests that transcription increases the rate at which TOP2 is processed by the proteasome (*Canela et al., 2019*). It has also been reported that TDP2, with the co-operation of secondary cofactors, can resolve unprocessed TOP2ccs in a proteasome-independent manner (*Schellenberg et al., 2017*).

An alternate, more error-prone mechanism for TOP2cc removal is mediated by MRE11 endonucleolytic cleavage in the vicinity of a trapped TOP2cc, which releases the entire TOP2 DNA-protein complex that results in the loss of small stretches of DNA (*Hoa et al., 2016; Lee et al., 2012*). Either of these mechanisms are able to produce protein-free DNA breaks that can then be recognized and

repaired by the major cellular DSB repair pathways: non-homologous end joining (NHEJ) and homologous recombination (HR).

It has long been recognized that trapped TOP2ccs are intrinsically reversible upon ETO washout (*Hsiang and Liu, 1989; Long et al., 1985*). Consistently, we observed that inhibiting the proteasome prior to ETO treatment enhanced the number of rapidly reversible ETO-stabilized TOP2ccs across the genome (*Canela et al., 2019*). Other studies have shown that inhibiting the proteasome not only preserves the reversibility of TOP2ccs but also is able to suppress DDR signaling (*Mao et al., 2001; Zhang et al., 2006*). However, the implications of suppressing the DDR in response to ETO using proteasome inhibitors, on both the long-term genome integrity and the overall viability of the cell, have not been fully explored. Considering that both proteasome inhibitors and topoisomerase poisons are used, sometimes in tandem, as frontline chemotherapeutic agents to treat a variety of cancers (*Cowell and Austin, 2012; Dittus et al., 2018; Manasanch and Orłowski, 2017; Thomas et al., 2017*), understanding how TOP2cc reversibility may impact the effectiveness of these drugs is clinically relevant.

Here, we utilize high-resolution genome-wide mapping of DSBs by END-seq (*Canela et al., 2016*) to examine the impact of proteasome inhibition on the fate of TOP2ccs. We found that once ETO-stabilized TOP2ccs had been proteolytically processed throughout the genome, and a robust DDR had been initiated, the large number of newly generated protein-free DSBs were repaired in a highly error-prone manner, resulting in toxic chromosomal translocations and rearrangements that led to cell death. Notably, the major DSB repair pathways (NHEJ and HR) contribute to the mis-repair of ETO-induced DSBs following proteasomal processing. By inhibiting proteasome-mediated degradation of TOP2ccs either through chemical inhibition or by ablation of RNF4-mediated ubiquitination of TOP2ccs, an intact and enzymatically competent TOP2 was able to re-seal the protein-linked DSBs without invoking a significant DDR. As a result, cells were protected from genomic instability, which ultimately led to enhanced cell survival after treatment with topoisomerase poisons.

Results

Proteasomal activity is necessary for triggering a DNA damage response following ETO treatment

Building on previous observations that proteasome inhibition can specifically attenuate the induction of γ -H2AX by ETO (*Mao et al., 2001; Zhang et al., 2006*), we sought to first confirm these findings in mouse primary splenic B-cells. Since ETO stabilizes both TOP2A and TOP2B isoforms, resting B-cells were activated with cytokines for 12 hr (*Figure 1A*). This short-term treatment ensures that B-cells remain in G1 where only the TOP2B isoform is expressed (*Canela et al., 2017*). This treatment regime, therefore, allows us to minimize any differential effect of ETO on each isoform (*Errington et al., 2004; Willmore et al., 1998*) and to bypass essential TOP2-dependent processes, such as DNA replication.

In agreement with other studies (*Mao et al., 2001; Zhang et al., 2006*), we found that treatment with a high (50 μ M) dose of ETO for 2 hr elicited a strong γ -H2AX response in B-cells (*Figure 1B*). Pre-incubating cells with proteasome inhibitors (10 μ M MG132, 10 μ M Bortezomib (BTZ), 2 μ M Epoxomicin (EPN), or 10 μ M Ixazomib (IXA)) for 1 hr prior to ETO treatment almost completely abolished the γ -H2AX signal (*Figure 1B*). The suppressed γ -H2AX signal occurred specifically in response to ETO, as pre-treating cells with the same dose of proteasome inhibitor did not affect the γ -H2AX response to ionizing γ -irradiation (5 Gy IR) (*Figure 1B and C*). Thus, proteasomal activity is required for triggering a robust DDR specifically in response to ETO treatment.

Proteasome inhibition promotes the accumulation of reversible TOP2ccs

As trapped TOP2ccs are subjected to proteasomal degradation, unprocessed TOP2ccs accumulate on DNA in cells pre-treated with a proteasome inhibitor compared to cells treated with ETO alone (*Lee et al., 2016*). To confirm that proteasome inhibitors were having the same effect in our experimental system, we quantified TOP2ccs using the ICE assay (*Anand et al., 2018*) in ETO-treated primary B-cells pre-incubated with or without BTZ. In the presence of ETO, TOP2ccs were readily detected on DNA (*Figure 1D*). Immediately after ETO was washed out, however, the amount of

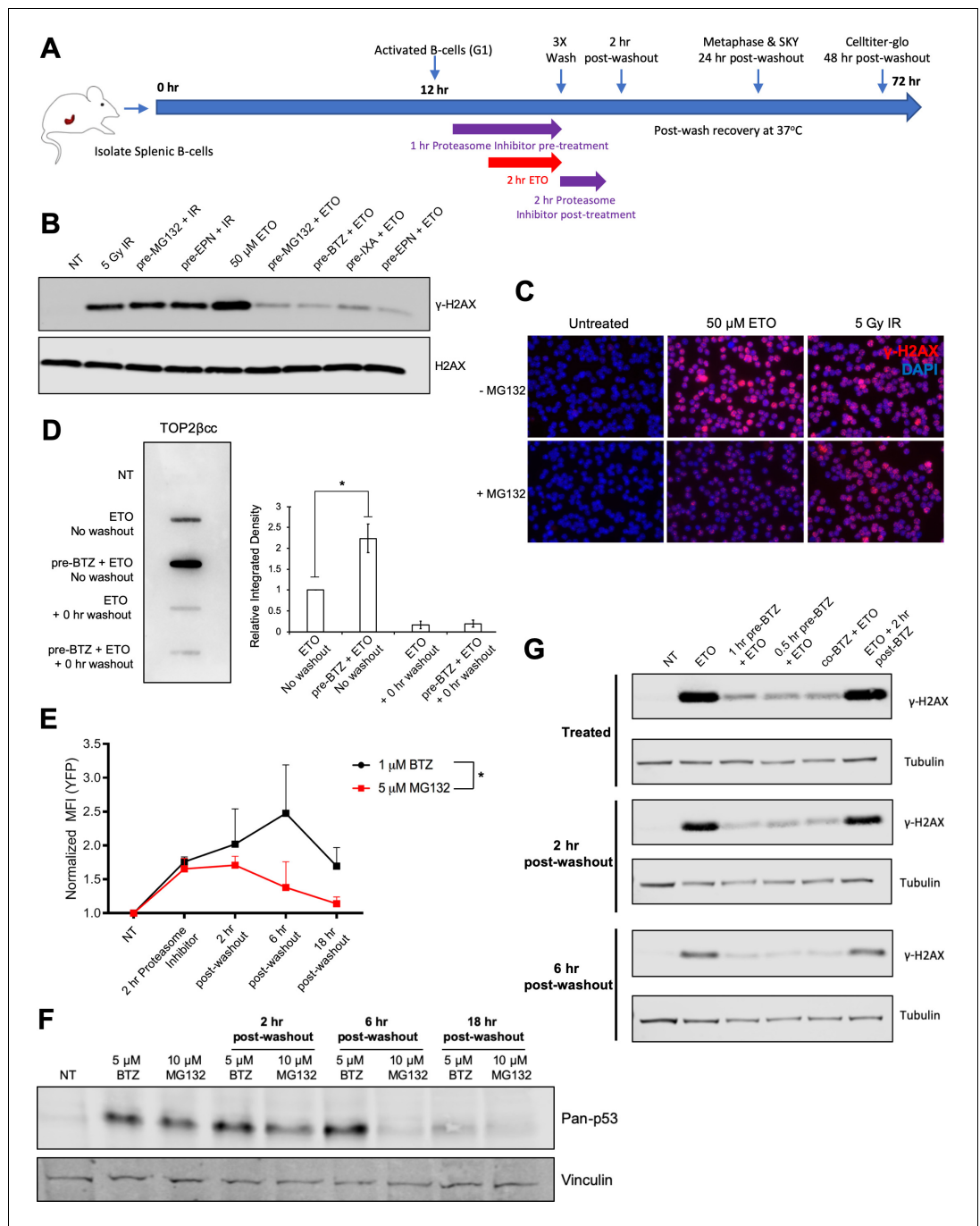


Figure 1. Proteasome machinery is essential for triggering DNA damage response to ETO treatment. (A) As indicated in the schematic, primary splenic B-cells were isolated from mouse spleens and activated with a cocktail of Il-4, LPS, and RP105. 12 hr post-activation, while the B-cells were still in the G1 phase of the cell cycle, they were pre-treated with proteasome inhibitor (10 μM MG132 or 5 μM Bortezomib) for 1 hr prior to an additional 2 hr co-treatment with 50 μM ETO. Following the ETO pulse, the cells were washed with ice cold drug-free media (3 × 5 min spin at 1500 rpm and 4°C to pellet B-cells between washes; 15–20 min total time to complete washout), then returned to fresh drug free media and allowed to recover at 37°C for up to 48 hr. In the case of post-treatment, proteasome inhibitor was added to the wash media and then the cells were incubated for an additional 2 hr at 37°C with proteasome inhibitor only. For western blot and ICE assay analysis, cells were harvested immediately following drug treatment or washout (0 hr washout). For metaphase and SKY analysis, cells were harvested 24 hr following washout. For CellTiter-Glo viability, cells were harvested 48 hr following washout. For END-seq analysis, cells were harvested before drug washout, immediately following washout (0 hr washout), or after a 2 hr recovery

Figure 1 continued on next page

Figure 1 continued

in drug free media (2 hr washout). (B) γ -H2AX western blot in G1 WT primary splenic B-cells following 2 hr 50 μ M ETO treatment \pm 1 hr proteasome inhibitor pre-treatment or 30 min following 5Gy IR \pm 1 hr proteasome inhibitor pre-treatment. Proteasome inhibitors tested: 10 μ M MG132, 10 μ M BTZ (Bortezomib), 2 μ M EPN (Epoxomicin), 10 μ M IXA (Ixazomib). (C) γ -H2AX immunofluorescence staining (red) in G1 arrested WT pre B cells following 2 hr, 50 μ M ETO treatment \pm 1 hr 10 μ M MG132 pre-treatment or 30 min after 5 Gy IR treatment \pm 1 hr 10 μ M MG132 pre-treatment. (D) WT primary splenic B-cells (N = 3) in G1 were treated for 2 hr with 50 μ M ETO \pm 1 hr, 5 μ M BTZ pre-treatment. DNA was then isolated from cells following the ICE assay protocol and probed with anti-TOP2 β antibody to quantify levels of TOP2 β cc. Relative band intensity was measured for each sample and averaged for all three mice (ETO vs. pre-BTZ + ETO p=0.0168; ETO vs. ETO + 0 hr washout p=0.0045; pre-BTZ + ETO vs. pre-BTZ + ETO 0 hr washout p=0.0046; statistical significance calculated using student T-test). (E) eHAP cells were transfected for 48 hr with a YFP-tagged degnon construct, which is degraded in a proteasome-dependent manner (Bence et al., 2001). Cells were then treated with 5 μ M MG132 or 1 μ M BTZ for 2 hr and then the drugs were washed out (3X wash in cold drug free media). Cells were fixed before washout with drugs still present or at 2 hr, 6 hr, and 18 hr post-washout. YFP signal intensity was quantified by FACS. (BTZ (before washout) vs. NT p=0.025; 2 hr post-washout MG132 vs NT p=0.049; statistical significance calculated using student T-test. MG132 vs BTZ p=0.038; statistical significance calculated using two column ANOVA). (F) pan-p53 levels in primary splenic B-cells treated for 3 hr with 10 μ M MG132 or 5 μ M BTZ. Drugs were then washed out and samples collected before washout or at 2 hr, 6 hr and 18 hr post-washout. (G) γ -H2AX levels in primary splenic B-cells as determined by Western blotting. Cells were treated with 50 μ M ETO for 2 hr \pm 1 hr or 30 min pre-treatment, co-treatment and post-treatment with 5 μ M BTZ at three different timepoints: before washout (treated), 2 hr and 6 hr post-washout.

DNA-bound TOP2 diminished strongly (Figure 1D). The proteasome continuously degraded ETO-trapped TOP2ccs, as evidenced by the markedly enhanced accumulation of TOP2ccs when cells were pre-incubated with BTZ (Figure 1D). The majority of these TOP2ccs also dissociated from DNA immediately following ETO washout (Figure 1D). Thus, inhibiting proteasomal degradation appears to preserve the integrity of TOP2ccs enabling reversal of complexes by completion of the enzymes' catalytic cycle upon drug removal.

Alternatively, proteasome activity could recover immediately after the removal of ETO and the proteasome inhibitor and would similarly lead to a loss of TOP2cc signal in the ICE assay. To determine the duration and reversibility of proteasomal inhibition, we directly monitored proteasome activity in eHAP cells transfected with a YFP-Degron reporter that has been demonstrated to be a *bona fide* proteasomal substrate (Bence et al., 2001). As expected, a 2 hr treatment with MG132 or BTZ significantly increased the YFP signal from baseline (Figure 1E). Following washout of MG132 or BTZ, the elevated YFP signal persisted for several hours before it began to decrease and BTZ appeared to be a more potent and persistent inhibitor of the proteasome than MG132 (Kisselev and Goldberg, 2001). As an additional measure of proteasome activity, we quantified the protein levels of p53, as it is known to be stabilized upon proteasome inhibition (An et al., 2000; Halasi et al., 2014). Consistent with the YFP-degron results in eHAP cells, we observed that p53 protein remained stabilized in primary B-cells for several hours after proteasome inhibitors were washed out, with BTZ again being more potent than MG132 (Figure 1F).

Thus, proteasome activity is not readily recovered even after the removal of proteasome inhibitor, suggesting that the rapid loss of ETO-induced TOP2ccs in MG132 pre-treated cells upon washout most likely reflects the reversal of TOP2ccs by completion of the enzymes' catalytic cycle upon drug removal. Accordingly, we did not observe a delayed γ -H2AX induction at either 2 hr or 6 hr post-ETO and BTZ washout, suggesting that proteasomal activity remain suppressed for at least several hours post-washout (Figure 1G). These data imply that persistent proteasome inhibition allows for TOP2cc reversal and prevents trapped TOP2ccs from being converted into protein-free DSB ends that are capable of eliciting a robust DNA damage response (DDR).

Timing of proteasome inhibition determines its impact on TOP2 metabolism

Contrary to our observations, previous studies have shown that proteasome inhibitors synergize with topoisomerase poisons like ETO in mediating cell killing (Aras and Yerlikaya, 2016; Ceruti et al., 2006; Destanovic et al., 2018; Dittus et al., 2018; Lee et al., 2016; von Metzler et al., 2009). Interestingly, we found that the addition of BTZ prior to or concurrent with ETO suppressed DDR

signaling, but incubating B-cells with BTZ post-ETO treatment did not (**Figure 1G**). These results showed that the timing of proteasome inhibitor treatment relative to ETO treatment is critical to its effects on TOP2cc metabolism and subsequent DDR signaling.

Proteasome inhibition decreases the persistence of ETO-induced TOP2-mediated DSBs by promoting TOP2cc reversibility

To further analyze the influence of the proteasome on TOP2ccs, we employed genome-wide DSB mapping by END-seq (*Canela et al., 2019; Canela et al., 2016*). While ETO can generate high levels of both SSBs and DSBs (*Baranello et al., 2014; Gittens et al., 2019*), END-seq only detects DSBs generated by ETO (*Canela et al., 2017; Canela et al., 2016*). However, this protocol allows us to capture and distinguish both TOP2ccs and protein-free DSBs generated by ETO (*Canela et al., 2019*). First, we assessed whether proteasome inhibition blocked TOP2 from making incisions in DNA. To this end, we used a cocktail of Exonuclease VII (ExoVII) and Exonuclease T (ExoT) during sample preparation, allowing us to capture all sites of TOP2 activity (*Canela et al., 2019*). As expected, END-seq analysis revealed that TOP2-mediated DSBs were readily detectable in ETO-treated B-cells (**Figure 2A–C**). The number and intensity of TOP2-mediated DSBs were reproducible across experiments (**Figure 2—figure supplement 1A–B**). Consistent with the results shown in **Figure 1D**, we found that BTZ pre-treatment did not dramatically affect the overall number or location of TOP2-mediated DSBs (**Figure 2A–C; Figure 2—figure supplement 1C–D**); TOP2-mediated DSBs were still strongly induced in the BTZ pre-treated sample, despite eliciting only a weak γ -H2AX response (**Figure 1B**). Thus, while proteasome inhibition does not affect the ability of TOP2 to cleave DNA, it helps maintain the resultant DSBs in a protein-linked form (persistent TOP2cc) that conceals them from the DDR. Nevertheless, we did observe a small decrease in the overall intensity of the TOP2-mediated DSB signal (**Figure 2A and C**) upon BTZ pre-treatment. This could be due to reversal of TOP2ccs in the BTZ pre-treated sample by completion of the enzymes' catalytic cycle upon drug removal.

Since inhibiting proteasomal degradation did not affect the initial formation of TOP2-mediated DSBs, we wanted to understand if proteasome inhibition affected their fate over time. To directly evaluate the impact of proteasome inhibition on repair of TOP2-mediated DSBs, we used END-seq to assess their longevity by harvesting primary B-cells both immediately following ETO/BTZ washout (0 hr washout) and after a 2 hr recovery in drug-free media at 37°C (2 hr washout). Notably, BTZ exerted a substantial impact on the rate at which TOP2-mediated DSBs resolved over the course of the 2 hr washout, with very few detectable breaks remaining after recovery relative to cells treated with ETO alone (**Figure 2A and D; Figure 2—figure supplement 1E**). We plotted the fraction of TOP2-mediated DSBs at each washout timepoint relative to the initial level of breakage following ETO treatment (**Figure 2D**). Using this analysis, we found that immediately following drug washout, 30% of the initial TOP2-mediated DSBs were still detectable in cells treated with ETO only, while just 15% were still present in the corresponding BTZ pre-treated sample (**Figure 2A and D**). After a 2 hr recovery, B-cells treated with ETO alone still had a detectable break signal (17%), whereas in BTZ-pretreated cells, it returned almost to baseline (4%, **Figure 2A and D**). This suggested that inhibiting the proteasome enhanced the amount of TOP2ccs which rapidly reverse following ETO washout.

As a second form of analysis, we normalized the TOP2-mediated DSB intensity at each post-washout timepoint. We introduced a new parameter, termed TOP2-mediated DSB persistence, which was calculated as the ratio of the peak intensity (RPKM) for individual TOP2-mediated DSBs at each timepoint (either 0 hr washout or 2 hr washout) relative to its initial intensity in the corresponding pre-washout sample (**Figure 2E; Figure 2—figure supplement 1F**). Through this analysis, we found that approximately 20% of the initial TOP2-mediated DSBs were classified as persistent immediately following ETO washout (0 hr washout), and 13% of initial TOP2-mediated DSBs were still persistent 2 hr post-washout (2 hr washout) (**Figure 2E**). By contrast, BTZ pre-treatment more significantly reduced the fraction of persistent TOP2-mediated DSBs both immediately following washout (~13%), as well as at 2 hr post-washout (~3.5%) (**Figure 2E**). These results, in conjunction with the ICE assay (**Figure 1D**), suggested that inhibiting the proteasome enhances TOP2cc reversal following ETO washout.

To directly measure the reversibility of TOP2ccs, we took advantage of the fact that ExoT lacks the ability to process protein-linked DSBs (persistent TOP2ccs that still have an intact 5'-

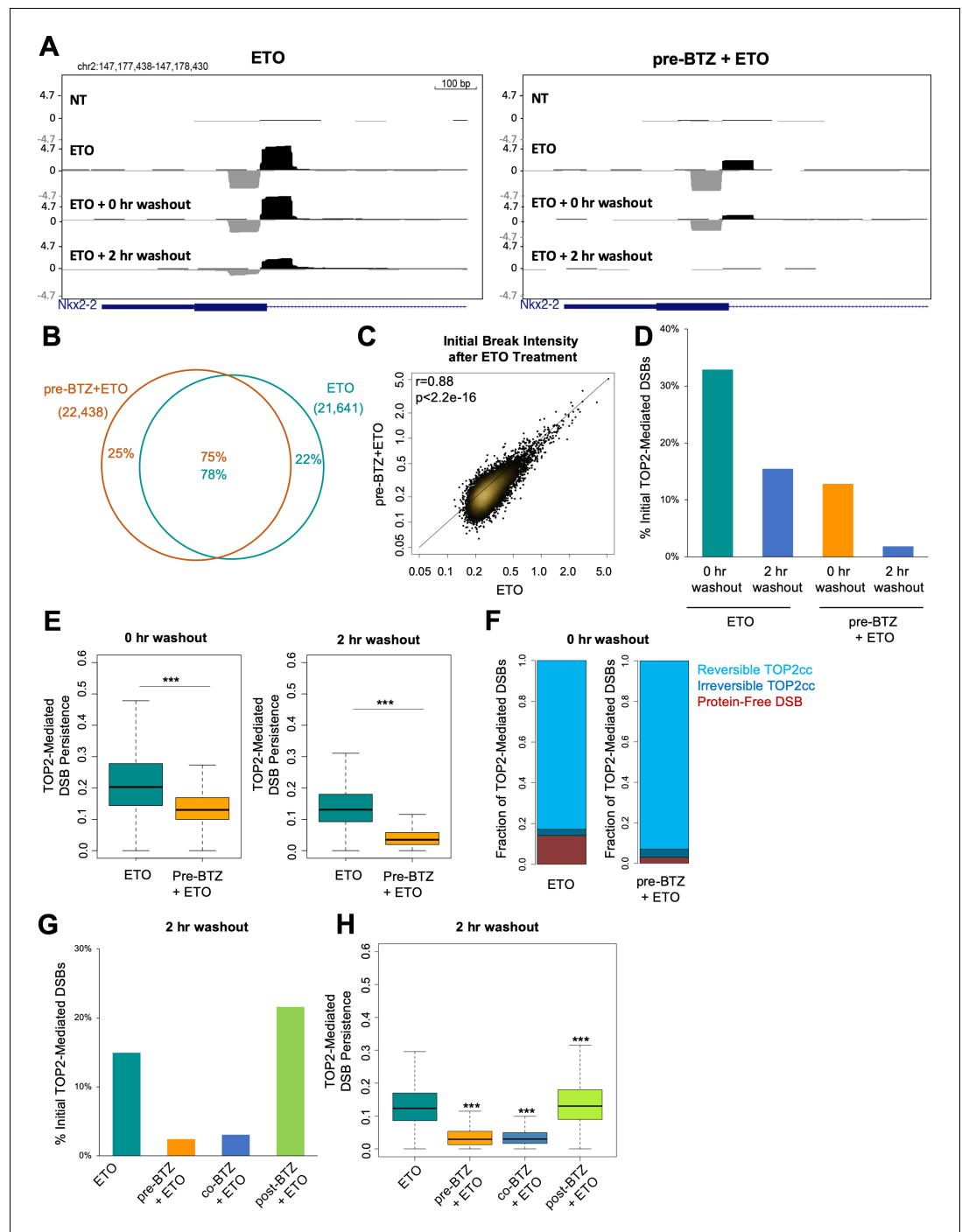


Figure 2. Proteasome inhibition decreases TOP2-mediated DSB persistence following ETO washout. (A) UCSC genome browser snapshot of a TOP2-mediated DSB captured within the Nkx2-2 gene locus by END-seq (ExoVII +ExoT) at three timepoints: in primary splenic B-cells treated for 2 hr with 50 μ M ETO \pm 1 hr 5 μ M BTZ pre-treatment, immediately following drug washout (0 hr washout), and at 2 hr post-washout (2 hr washout). (B) Venn diagram depicting the overlap between TOP2-mediated DSBs generated by ETO genome-wide in the 50 μ M ETO only sample (green) and the 5 μ M BTZ pre-treatment sample (orange). WT primary splenic B-cells were treated for 2 hr with 50 μ M ETO \pm 1 hr 5 μ M BTZ pre-treatment and processed by END-seq using ExoVII+ExoT. (C) Scatterplot depicting initial intensity of TOP2-mediated DSBs induced by ETO genome-wide in the 50 μ M ETO only sample vs. the 5 μ M BTZ pre-treatment sample (ETO vs. pre-BTZ + ETO $p<2.2e^{-16}$; statistical significance calculated by Pearson's correlation coefficient). WT primary splenic B-cells were treated for 2 hr with 50 μ M ETO \pm 1 hr 5 μ M BTZ pre-treatment. (D) Bar graph measuring the number of TOP2-mediated DSBs (END-seq with

Figure 2 continued on next page

Figure 2 continued

ExoVII+ExoT) at 0 hr and 2 hr post-washout timepoints, represented as a fraction of the initial number of TOP2-mediated DSBs generated genome-wide (% initial breaks after ETO treatment determined by peak calling). WT primary splenic B-cells were treated for 2 hr with 50 μM ETO treatment ± 1 hr 5 μM BTZ pre-treatment. (E) Box-plot of TOP2-mediated DSB persistence (relative intensity of initial breakage) genome-wide at 0 hr and 2 hr post-washout timepoints (left and right panels respectively). Green box 50 μM ETO only sample and orange box 5 μM BTZ pre-treatment sample (ETO vs. pre-BTZ + ETO $p < 2.2 \times 10^{-16}$, statistical significance calculated by student T-test). WT primary splenic B-cells were treated for 2 hr with 50 μM ETO treatment ± 1 hr 5 μM BTZ pre-treatment prior to washout. (F) Bar graph depicting the percentages of total TOP2-mediated DSBs (measured by ExoVII+ExoT), protein-free DSBs (measured by ExoT), and TOP2ccs (inferred by subtracting protein free DSBs from the levels of total TOP2-mediated DSBs). Reversible TOP2ccs (light blue), irreversible TOP2ccs (dark blue), and protein-free DSBs (red). WT primary splenic B-cells were treated for 2 hr with 50 μM ETO treatment ± 1 hr 5 μM BTZ pre-treatment. (G) Bar graph depicting the number of TOP2-mediated DSBs at 2 hr post-washout (END-seq with ExoVII+ExoT), represented as a fraction of the initial number of TOP2-mediated DSBs measured genome-wide (% initial breaks after ETO treatment determined by peak calling). WT primary splenic B-cells were treated for 2 hr with 50 μM ETO treatment \pm pre treatment, co-treatment, and post-treatment with 5 μM BTZ. Post treatment with BTZ was for 2 hr. (H) Box-plot depicting TOP2-mediated DSB persistence genome-wide at 2 hr post-washout ($p < 2.2 \times 10^{-16}$ for ETO vs. pre-BTZ + ETO, ETO vs co-BTZ + ETO, and ETO vs post-BTZ + ETO; statistical significance calculated by student T-test). WT primary splenic B-cells were treated for 2 hr with 50 μM ETO treatment \pm pre treatment, co-treatment, and post-treatment with 5 μM BTZ.

The online version of this article includes the following figure supplement(s) for figure 2:

Figure supplement 1. TOP2-Medated DSBs are reproducibly captured by END-seq.

phosphotyrosyl bond) and therefore allows for the detection of only protein-free (i.e. proteolytically processed) DSBs (Canela et al., 2019). As such, the levels of TOP2ccs can be estimated by the difference between total TOP2-mediated DSBs detected by ExoVII+ExoT and protein-free DSBs detected by ExoT alone (Canela et al., 2019). Our analyses revealed that 76% of TOP2-mediated DSBs reversed immediately following washout (0 hr washout), with the majority of remaining lesions being converted into protein-free DSBs (Figure 2F). The fraction of reversible TOP2ccs was even higher in the BTZ pre-treated cells, as 90% of the initial TOP2-mediated DSBs were reversible immediately following washout (Figure 2F). Thus, suppressing proteasomal degradation of TOP2ccs led to increased TOP2cc self-reversal.

Finally, we assessed how the timing of proteasome inhibition impacted the rate at which TOP2-mediated DSBs are resolved. We found that compared to ETO alone, both BTZ pre-treatment and co-treatment significantly reduced the number and persistence of TOP2-mediated DSBs after a 2 hr washout (Figure 2G and H). By contrast, BTZ post-treatment slightly increased the number, as well as persistence, of TOP2-mediated DSBs at the same timepoint (Figure 2G and H). These results confirmed that the timing of proteasome inhibition relative to ETO treatment determined its impact on the resolution of TOP2-mediated DSBs.

Inhibiting proteolytic degradation of TOP2ccs suppresses DNA end resection of TOP2-mediated DSBs

Since protein-free DSBs persist for a significant period of time following ETO washout, it enabled the study of DNA processing at these sites. We observed clear evidence of 5' to 3' DNA end-resection of TOP2-mediated DSBs immediately after drug washout (Figure 3A). After 2 hr post ETO treatment, the extent and intensity of resection had increased (Figure 3A), indicating ongoing end-processing at persistent TOP2-mediated DSBs. In ETO-treated cells pre-incubated with BTZ, while there were still low levels of protein-free DSBs present immediately following drug washout (0 hr washout), we could barely detect end-resection at individual breaks (Figure 3A). Genome-wide, we were able to identify 1289 resected breaks in ETO-treated cells immediately following washout, while only 496 resected breaks were detected in BTZ pre-treated cells, a 2.5-fold decrease (Figure 3B). The end-resection detected in ETO-treated cells genome-wide was reproducible across replicates (Figure 3—figure supplement 1). Therefore, inhibiting the proteolytic degradation of TOP2ccs prevented DNA repair-associated nucleases from processing TOP2-mediated DSBs. Moreover, the extent of resection, defined as the maximum distance away from the break summit, was significantly shorter in BTZ-pretreated cells compared to cells treated with ETO alone (Figure 3C;

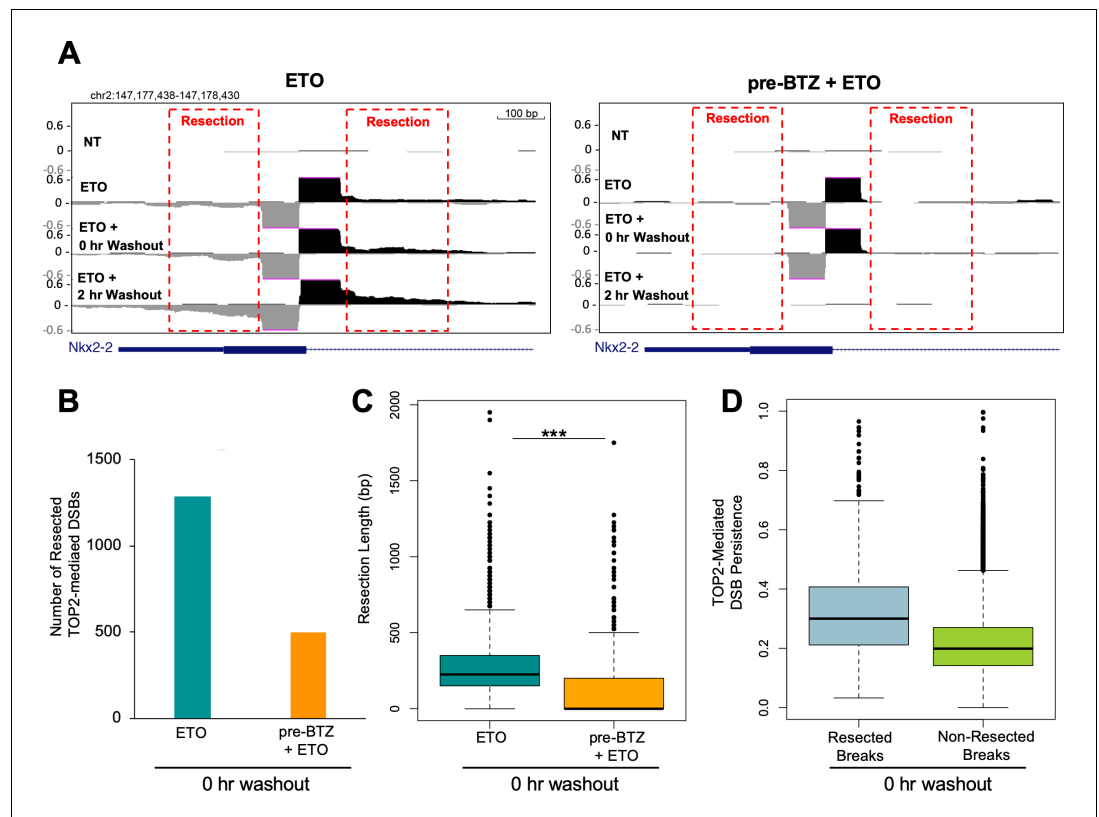


Figure 3. Proteasomal degradation of the TOP2cc is associated with DSB resection. (A) Zoomed in UCSC genome browser snapshot of the same TOP2-mediated DSB as in **Figure 2A** at three timepoints: 2 hr with 50 μ M ETO (ETO), immediately following drug washout (0 hr WO), and at 2 hr post-washout (2 hr WO) (left panel). In right panel, WT primary splenic B-cells were pre-treated for 1 hr with 5 μ M BTZ pre-treatment prior to washout. Red box indicates areas with resection signal. (B) Bar graph depicting the number of TOP2-mediated DSBs that had a resection signal immediately following drug washout (0 hr washout) in WT primary splenic B-cells treated for 2 hr with 50 μ M ETO \pm 5 μ M BTZ pre-treatment. Green bar- 50 μ M ETO only sample and orange bar- 5 μ M BTZ pre-treatment sample. (C) Box-plot quantifying maximum resection distance for all persistent TOP2-mediated DSBs genome-wide immediately following drug washout (0 hr washout) in WT primary splenic B-cells treated for 2 hr with 50 μ M ETO \pm 5 μ M BTZ pre-treatment. Green box 50 μ M ETO only sample and orange box 5 μ M BTZ pre-treatment sample (ETO vs. pre-BTZ + ETO $p < 2.2e^{-16}$; statistical significance calculated by student T-test). (D) Box-plot of resected (grey) and non-resected (green) TOP2-mediated DSBs genome-wide immediately following drug washout (0 hr washout) in WT primary splenic B-cells treated for 2 hr with 50 μ M ETO \pm 5 μ M BTZ pre-treatment. TOP2-mediated DSB resection values are plotted as a function of their persistence at the 0 hr washout timepoint. The online version of this article includes the following figure supplement(s) for figure 3:

Figure supplement 1. TOP2-Medated DSB resection is reproducibly captured by END-seq.

Figure 3—figure supplement 1B). Finally, we found that after ETO removal, TOP2-mediated DSBs undergoing nucleolytic processing (resected breaks) tended to be more persistent than non-resected breaks (**Figure 3D**; **Figure 3—figure supplement 1C**). Thus, the longer a TOP2-mediated DSB persists in the genome, the more likely it will be processed and repaired in a potentially error-prone manner.

Proteasome inhibitor pre-treatment prevents ETO-induced genome instability and cytotoxicity

Enzymatic reversal of TOP2ccs is predicted to be an error-free process. By contrast, the degradation of TOP2ccs followed by DSB repair is potentially more susceptible to error. Nevertheless, repair of ETO-induced DSBs by TDP2-dependent NHEJ might be performed with fidelity (**Gómez-Herreros et al., 2013**) since it involves simple re-ligation of compatible 4 bp overhangs. To directly

address this question, we exposed primary B-cells in G1 to ETO (2 hr, 50 μ M) with or without BTZ pre-treatment, or post-treatment. After washing out the drugs, cells were allowed to recover at 37°C in fresh, drug-free media for 24 hr before they were harvested for mitotic chromosome analysis (**Figure 1A**). Notably, we found that even a short pulse of ETO induced a substantial number and variety of chromosomal aberrations in WT B-cells (~14 aberrations per cell) (**Figure 4A and B**). The majority of aberrations that we observed were dicentric chromosomal fusions and chromosome breaks (**Figure 4A and B**). Post-treatment with MG132 did not mitigate the genotoxic effects of ETO (**Figure 4B**), consistent with the lack of effect it had on ETO-induced γ -H2AX response (**Figure 1G**). However, pre-treating B-cells with MG132 or BTZ completely protected cells from accruing chromosomal aberrations induced by ETO, with less than one aberration detected per cell (**Figure 4A and B**). Therefore, the repair of DSBs that arise from proteasome-mediated degradation of TOP2ccs is error-prone, while preventing TOP2cc processing preserves genome integrity.

Mitotic chromosome analysis is limited in its ability to determine the extent of chromosomal fusion events, as pieces of two or more chromosomes could be ligated together and still appear as a normal chromosome when stained with only DAPI. We consistently detected the presence of elongated chromosomes in mitotic spreads prepared from ETO-treated B-cells, suggesting that these might result from complex fusions involving multiple chromosomal fragments. To further characterize these seemingly intact long chromosomes, we performed spectral karyotyping (SKY) (*Liyanae et al., 1996*). As shown in **Figure 4C and D**, SKY analysis revealed that ETO-induced chromosomal fusions were extensive and complex. Indeed, these events resembled chromothripsis, in which fragments originating from three or more chromosomes are fused together (*Zhang et al., 2013*). Strikingly, pre-treating B-cells with MG132 before ETO completely protected them from all types of chromosomal fusions (**Figure 4C and D**). These results highlight the severe genotoxic consequences of a transient high dose pulse of ETO and demonstrate that such ETO-induced genome instability is proteasome-dependent.

Consistent with the impact of the proteasome on genome integrity, we found that pre-treatment with MG132, but not post-treatment, mitigated the induction of cell cycle arrest by ETO evidenced by the increased cellular incorporation of EdU after the start of ETO treatment (**Figure 4E**). While proteasome inhibition itself caused a reversible block on S-phase entry, as previously described (*Rastogi and Mishra, 2012*), proteasome inhibitor pre-treatment but not post-treatment, significantly diminished the cytotoxicity of ETO (**Figure 4F**). Taken together, our data indicate that proteasome inhibitor pre-treatment maintains cellular proliferative capacity and long-term viability by blocking ETO-induced genome instability.

Misrepair of DSBs following TOP2 degradation is mediated by multiple DNA repair pathways

To determine if DDR signaling per se is responsible for the error-prone repair of TOP2-associated DSBs, we conducted mitotic spread analyses in *ATM*^{-/-} and *H2AX*^{-/-} primary B-cells. We found that these DDR signaling deficient mutants accumulated somewhat higher levels of chromosomal aberrations following ETO treatment compared to WT (**Figure 5A**). Importantly, proteasome inhibitor pre-treatment almost completely abolished ETO-induced damage in WT, as well as in *ATM*^{-/-} and *H2AX*^{-/-} B-cells (**Figure 5A**). Thus, proteasome inhibition but not ATM- γ -H2AX driven DDR signaling protects against ETO-induced genome instability.

Both NHEJ and HR are thought to contribute to the repair of ETO-induced DSBs (*Ledesma et al., 2009; Gómez-Herrerros et al., 2013; Gómez-Herrerros et al., 2017; Hoa et al., 2016; Pommier et al., 2016*). To determine whether classical NHEJ or HR is primarily responsible for the misrepair of DSBs, we tested primary B-cells deficient in the key end joining factor DNA ligase IV (*Lig4*^{-/-}) or the key HR factors BRCA1 (*BRCA1* ^{Δ 11}) and BRCA2 (*BRCA2*^{-/-}). To this end, primary resting (G0) *Lig4*^{-/-}, *BRCA1* ^{Δ 11} and *BRCA2*^{-/-} B-cells were first activated with cytokines for 12 hr and 24 hr to drive G1- or S-phase entry, respectively, at which point they were exposed to ETO. After ETO was washed out, B-cells were given an additional 24 hr to recover before mitotic spread analysis. We found that loss of *Lig4*, *BRCA1* or *BRCA2* failed to mitigate aberrant chromosomal rearrangements in ETO-treated G1 and cycling B-cells, respectively (**Figure 5B and C; Figure 5—figure supplement 1**). Furthermore, MG132 pre-treatment completely prevented ETO-induced genome instability in *Lig4*^{-/-} and *BRCA1* ^{Δ 11} cells (**Figure 5B and C**). Thus, the protective effects of

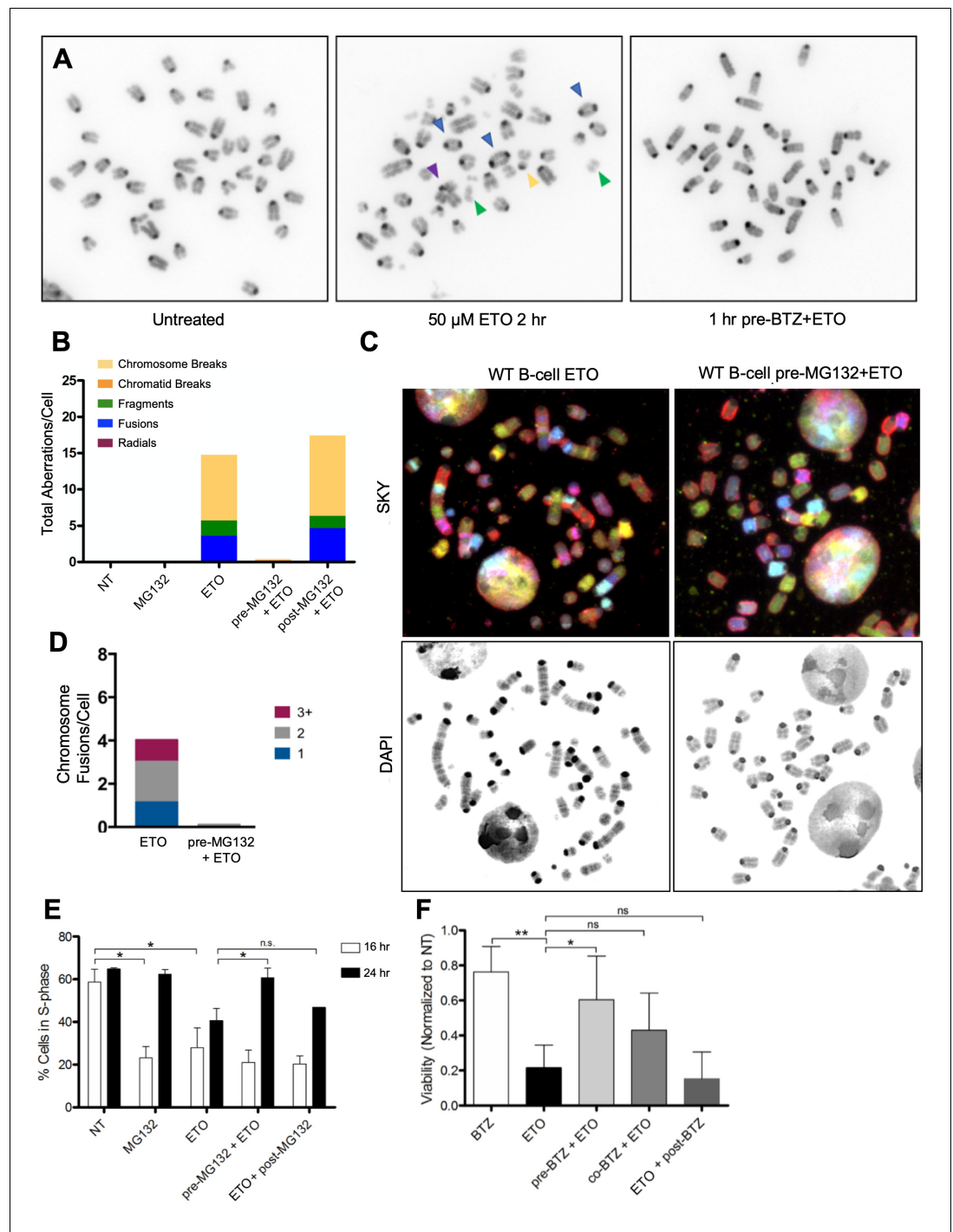


Figure 4. Proteasome inhibition suppresses ETO-induced genome instability and improves cell survival. (A) Example of mitotic spreads from WT primary splenic B-cells treated for 2 hr in G1 with 50 μ M ETO \pm 1 hr 5 μ M BTZ pre-treatment, followed by 24 hr recovery in drug free medium prior to harvesting metaphases. Colored arrows indicate the type of aberrations as quantified and described in B. (B) Analysis of chromosomal aberrations (Chromosome Breaks (yellow), Chromatid Breaks (orange), Fusions (blue), Radials (purple) and Fragments (green)). 50 metaphases were counted for each condition. (C) Example of mitotic spreads from WT primary splenic B-cells treated for 2 hr in G1 with 50 μ M ETO \pm 1 hr 10 μ M MG132 pre-treatment, and then harvested 24 hr after washout for Spectral Karyotyping Analysis (SKY) (Left and right top panels). SKY reveals more complex fusions involving multiple chromosomes, compared to the fusions observable by DAPI staining only (Left and right bottom panels). (D) Analysis of chromosomal fusion determined by SKY analysis. Chromosome fusions were counted in 35 mitotic

Figure 4 continued on next page

Figure 4 continued

spreads per condition and were broken down by how many chromosomes were involved (1, two or greater than 3 (+)) per fusion event per cell. (E) Quantification of percent cells in S phase determined by FACS. WT primary splenic B-cells were treated in G1 for 2 hr with 50 μ M ETO \pm 1 hr 10 μ M MG132 pre-treatment. 16 or 24 hr after washout, cells were pulsed for 30 min with EdU pulse and analyzed by FACS (16 hr NT vs MG132 $p=0.012$; 16 hr NT v ETO $p=0.0485$; 24 hr ETO vs pre-MG132 + ETO $p=0.049$; 24 hr ETO vs. post-MG132 $p=0.46$; statistical significance calculated by student T-test). (F) Viability of WT primary splenic B-cells as determined using the CellTiter-Glo luminescence assay 48 hr following 2 hr of 50 μ M ETO treatment \pm pre treatment, co-treatment, or post-treatment with 5 μ M BTZ (BTZ v ETO $p=0.0006$, ETO v pre-BTZ + ETO $p=0.015$, statistical significance calculated by student T-test). During treatment cells were in the G1 phase of the cell cycle.

proteasome inhibition on ETO-induced genome instability is not cell cycle dependent, and neither

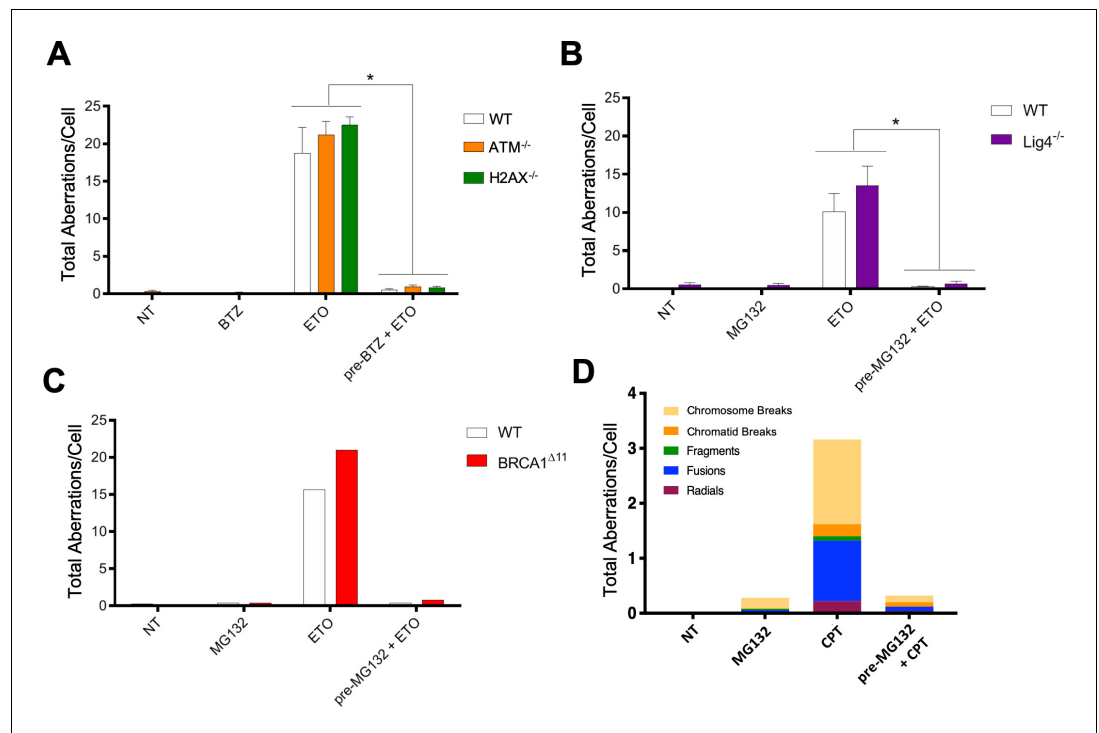


Figure 5. Multiple DNA repair pathways contribute to ETO-induced genome instability. (A) Mitotic spread analysis of WT (White), *ATM*^{-/-} (Orange), and *H2AX*^{-/-} (Green) primary splenic B-cells treated in G1 for 2 hr with 50 μ M ETO \pm 1 hr 5 μ M BTZ pre-treatment. B-cells were fixed for mitotic spread analysis following a 24 hr recovery at 37 $^{\circ}$ C in drug free media. Total chromosomal aberrations were counted in 50 metaphases (N = 3) and averaged for each genotype. (ETO vs. pre-BTZ + ETO: WT, $p=0.006$; *ATM*^{-/-}, $p=0.0004$; *H2AX*^{-/-}, $p<0.0001$; statistical significance calculated by student T-test). (B) Mitotic spread analysis of WT (White) and *Lig4*^{-/-} (Purple) primary splenic B-cells treated in G1 for 2 hr with 50 μ M ETO \pm 1 hr 10 μ M MG132 pre-treatment. B-cells were fixed for mitotic spread analysis following a 24 hr recovery at 37 $^{\circ}$ C in drug free media. Total chromosomal aberrations were counted in 50 metaphases (N = 3) and averaged for each genotype. (ETO vs pre-MG132 + ETO: WT, $p=0.0154$; *Lig4*^{-/-}, $p=0.0075$; statistical significance calculated by student T-test). (C) Mitotic spread analysis of cycling (24 hr post-activation) WT (White) and *BRCA1*^{A11} (Red) primary splenic B-cells treated for 2 hr with 50 μ M ETO \pm 1 hr 10 μ M MG132 pre-treatment. B-cells were fixed for mitotic spread analysis following a 24 hr recovery at 37 $^{\circ}$ C in drug free media. Total chromosomal aberrations were counted in 50 metaphases per condition. (D) Mitotic spread analysis of cycling primary splenic B-cells treated for 2 hr with 12.5 μ M CPT \pm 1 hr 10 μ M MG132 pre-treatment. B-cells were fixed for mitotic spread analysis following a 24 hr recovery at 37 $^{\circ}$ C in drug free media. Total chromosomal aberrations were counted in 50 metaphases per condition. The online version of this article includes the following figure supplement(s) for figure 5:

Figure supplement 1. Multiple DNA repair mechanisms contribute to error-prone repair of ETO-induced damage.

classical NHEJ nor HR appears to be strictly required to generate ETO-induced chromosomal aberrations.

Given the lack of clear dependency on canonical DSB repair pathways, we next explored whether Pol θ -mediated alternative end joining could be a major contributor of ETO-induced genome instability. Similar to Lig4- and BRCA1/2-deficiency, however, loss of Pol θ (POLQ^{-/-}) did not significantly attenuate the formation of complex chromosomal rearrangements in ETO-treated cells (**Figure 5—figure supplement 1**). Therefore, multiple DNA repair mechanisms likely contribute to the error-prone repair of ETO-induced DSBs.

Proteasome inhibitor pre-treatment prevents degradation of TOP1 cleavage complexes and camptothecin-induced genome instability

In addition to preventing the degradation of TOP2ccs, previous studies have shown that proteasome inhibitors are able to suppress ATM- γ -H2AX signaling in response to damage induced by TOP1 poisons like Camptothecin (CPT) (**Lin et al., 2008**), which stabilizes TOP1ccs in the same mechanistic way ETO stabilizes TOP2ccs (**Pommier et al., 2016**). We, therefore, assessed if cells pre-treated with proteasome inhibitors were protected from chromosomal aberrations caused by CPT. Our results showed that MG132 pre-treatment largely suppressed CPT-induced chromosomal aberrations (**Figure 5D**), similar to its effects in ETO-treated cells (**Figure 5A–C**). Thus, inhibiting the proteolytic degradation of either TOP1ccs or TOP2ccs prevents subsequent DNA mis-repair that leads to genome instability.

The SUMO-targeted ubiquitin ligase RNF4 promotes proteasome-mediated processing of TOP2ccs

Based on the results presented above, it is clear that the degradation of ETO-stabilized TOP2ccs leads to genome instability, while chemical suppression of proteasomal TOP2cc degradation prevents the accumulation and mis-repair of genotoxic DSBs. Recent work has described a SUMO-ubiquitin (Ub) pathway that recognizes DNA-bound topoisomerase-DNA complexes, wherein the SUMO-targeted E3 ubiquitin ligase (STUbL) RNF4 ubiquitinates TOP2 leading to its degradation (**Sun et al., 2019**). We therefore assessed whether interfering with the cell's ability to sense and recruit the proteasome to trapped TOP2ccs would confer a chemo-protective effect similar to cells treated with BTZ and ETO (**Figure 1B, Figure 4A–F**). To this end, we treated WT and RNF4^{-/-} MEFs (**Hu et al., 2010**) with 10 μ M ETO for 1 hr with or without BTZ pre-incubation (1 μ M, 1 hr), and probed for γ -H2AX. ETO produced a weakened γ -H2AX response in RNF4^{-/-} MEFs compared to WT MEFs (**Figure 6A**), suggesting that RNF4 facilitates proteasomal degradation of TOP2ccs, which in turn generates γ -H2AX. Notably, while BTZ pre-treatment suppressed the ETO-induced γ -H2AX response in WT MEFs (**Figure 6A**), it did not further reduce the γ -H2AX response in RNF4^{-/-} MEFs (**Figure 6A**), suggesting that RNF4 is epistatic with the proteasome with regard to TOP2cc degradation. To explore this further, we used END-seq to quantify the number and intensity of TOP2-mediated DSBs in ETO treated RNF4^{-/-} and WT primary B-cells. Our results showed that there was a 6-fold reduction of protein-free DSBs detected by END-seq in RNF4^{-/-} B-cells compared to WT (**Figure 6B**, top right), while the initial levels of total TOP2-mediated DNA cleavage were similar between the genotypes (**Figure 6B**, top left). This effect was comparable to what we observed by chemically inhibiting the proteasome with BTZ, which reduced the number of protein-free DSBs by ~5 fold (**Figure 6B**, bottom right). These results indicate that RNF4 ubiquitination is critical for proteasome-mediated processing of TOP2ccs into genotoxic protein-free DSBs.

To assess if the loss of RNF4 conferred resistance to ETO, we determined how RNF4 deletion affected short-term cellular viability and long-term colony formation potential in ETO-treated B-cells and MEFs, respectively. We found that RNF4^{-/-} cells were significantly more viable and retained higher colony formation capacity after a 1 hr pulse of ETO compared to WT counterparts (**Figure 6C and D**). Consistent with increased viability, RNF4^{-/-} B-cells accumulated 60% less chromosomal aberrations after ETO treatment compared to WT B-cells (**Figure 6E**). Taken together, these results indicated that impairing the proteasome response to trapped TOP2ccs reduces the cytotoxicity and genotoxicity of ETO. Notably, pre-treating RNF4^{-/-} B-cells with BTZ further reduced aberrant chromosomal repair (**Figure 6E**), suggesting that RNF4-mediated ubiquitination is likely not the only mechanism by which the proteasome is recruited to TOP2ccs.

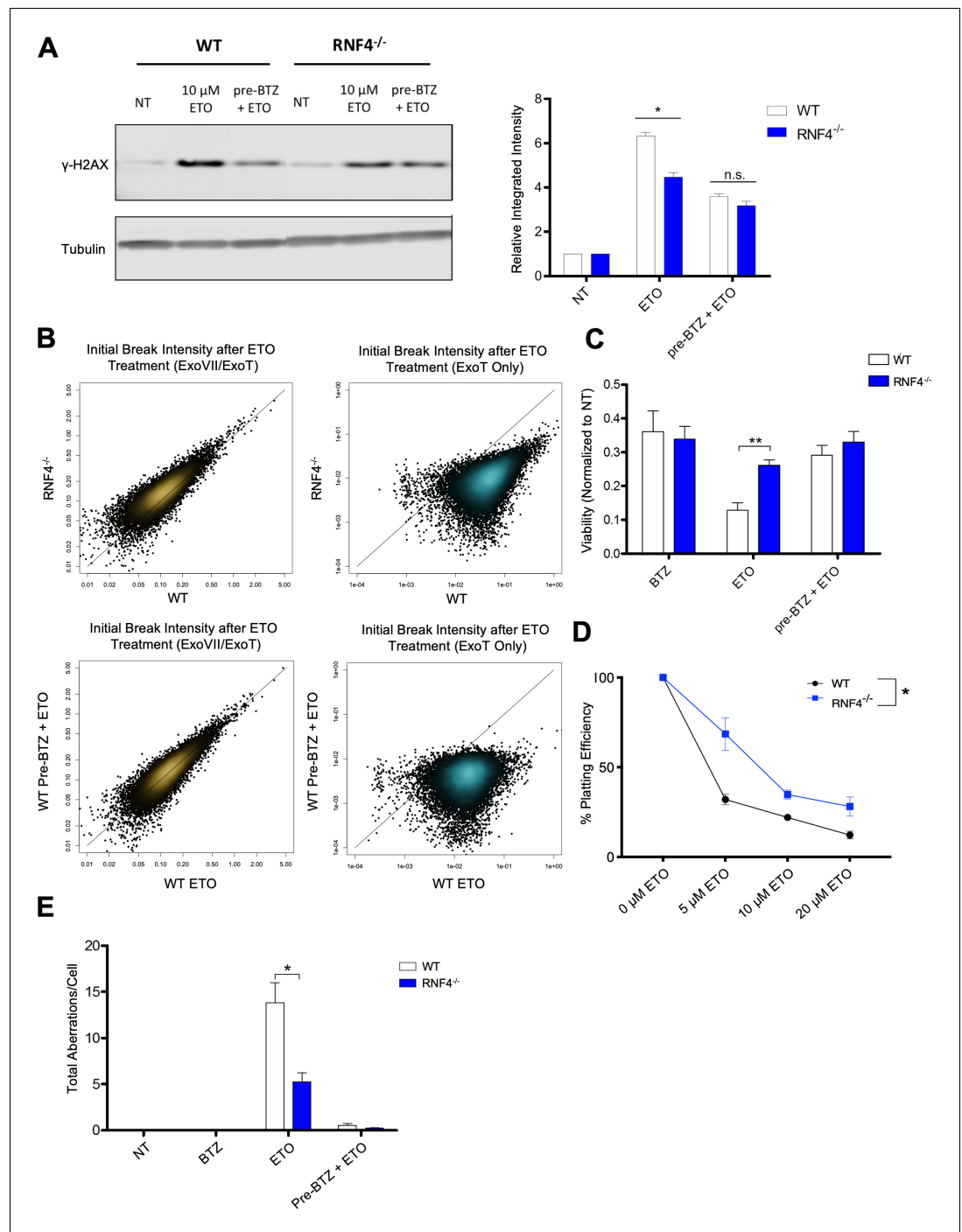


Figure 6. The SUMO-targeted Ubiquitin-Ligase RNF4 functions in proteasome mediated processing of TOP2cc. (A) Example γ -H2AX western blot in WT and RNF4^{-/-} MEFs treated with 10 μ M ETO for 1 hr \pm 1 hr 1 μ M BTZ pre-treatment (Left Panel). Bar graph quantifying the relative band intensity from γ -H2AX western blots (N = 3) of WT (White) and RNF4^{-/-} (Blue) MEFs treated with 10 μ M ETO (Right Panel). (WT ETO vs RNF4^{-/-} ETO p=0.0018; statistical significance calculated by student T-test). (B) Scatterplots depicting initial intensity of all TOP2-mediated DSBs (ExoVII/ExoT, Top Left) and initial intensity of protein-free DSBs genome-wide (ExoT, Top Right) induced by 2 hr treatment of WT and RNF4^{-/-} B cells with 50 μ M ETO. Scatterplots of all TOP2-mediated DSBs (ExoVII/ExoT, Bottom Left) and protein-free DSBs genome-wide (ExoT, Bottom Right) in WT primary splenic B-cells treated with 50 μ M ETO only vs. 50 μ M ETO + 5 μ M BTZ pre-treatment. (C) Viability of WT (White) and RNF4^{-/-} (Blue) primary splenic B-cells, as determined by the CellTiter-Glo luminescence assay 48 hr following 2 hr 50 μ M ETO treatment \pm 1 hr 5 μ M BTZ pre-treatment. (D) Colony formation assay in WT (White) and RNF4^{-/-} (Blue) MEFs. Cells

Figure 6 continued on next page

Figure 6 continued

were seeded in 6 cm plates at 100, 1000 and 10000 cells/plate and pulsed with 5–20 μM ETO for 1 hr and then left to recover and form colonies for 7 days. The number of colonies from duplicate plates were averaged and plotted at each concentration (N = 3) (WT vs RNF4 $p=0.0034$; statistical significance calculated by ANOVA). (E) Mitotic spread analysis of WT (White) and RNF4^{-/-} (Blue) primary splenic B-cells treated in G1 for 2 hr with 50 μM ETO \pm 1 hr 5 μM BTZ pre-treatment. B-cells were fixed for mitotic spread analysis following a 24 hr recovery at 37°C in drug free media. Total chromosomal aberrations were counted in 50 metaphases (N = 3) and averaged for each genotype. (WT vs. RNF4^{-/-} ETO: $p=0.048$, statistical significance calculated by student T-test).

Discussion

In this study, we describe a mechanism by which ETO-induced genotoxicity can be abolished by inhibiting proteasome mediated degradation of TOP2 cleavage complexes (TOP2ccs). In the absence of proteolytic degradation, TOP2 remains enzymatically competent and is able to reseal the protein-linked DSB without invoking a DNA damage response (DDR). However, once degradation commences, a TOP2cc is no longer reversible, and the previously hidden DSB become unmasked, triggering a potent DDR signaling response. Following degradation of a TOP2cc, the resultant protein free DSBs appear to engage multiple repair pathways, including error-free NHEJ (Gómez-Herreros et al., 2013; Gómez-Herreros et al., 2017; Figure 7A). However, due to the large number of lesions induced by ETO, many DSBs remain unrepaired or mis-repaired which can destabilize the genome. In contrast, by preventing proteasome-mediated unmasking of TOP2-mediated DSBs,

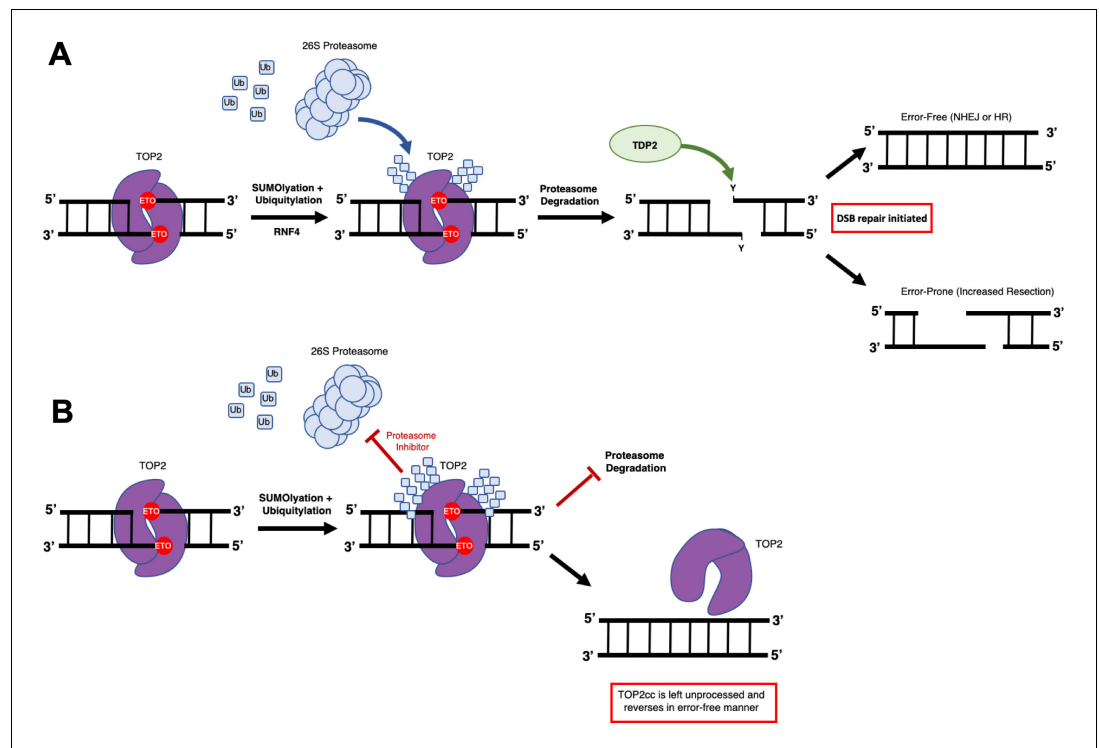


Figure 7. Model of proteasome mediated repair of TOP2ccs. (A) ETO-stabilized TOP2ccs are targeted for proteasomal degradation by the 26S proteasome via both SUMOylation and Ubiquitination, mediated by the SUMO-targeting ubiquitin ligase RNF4 and possibly other enzymes. Upon degradation of the TOP2 protein within the TOP2cc, the remaining 5'-phosphotyrosyl bonds must be processed by TDP2, generating clean protein-free DSBs with overhangs that can be repaired in a manner that is not always error-free. (B) If the proteasome is not recruited due to loss of RNF4-mediated TOP2cc polyubiquitylation or its activity is inhibited chemically, the TOP2cc is not recognized by the DNA repair machinery and the TOP2 protein retains full enzymatic ability to reverse itself once ETO is washed out.

error-prone repair is not engaged, thereby facilitating the reversal of TOP2ccs through completion of the enzymes' catalytic cycle upon drug removal, and preserving genome integrity (**Figure 7B**).

Both proteasome inhibitors (e.g. BTZ) and topoisomerase poisons (e.g. ETO, doxorubicin) are used clinically as therapeutic anti-cancer agents, sometimes in combination (**Cowell and Austin, 2012; Dittus et al., 2018; Manasanch and Orlowski, 2017; Nitiss, 2009b; Palumbo et al., 2008; Thomas et al., 2017**). Notably, prior studies have shown that proteasome inhibitors potentiate the cytotoxicity of TOP2 poisons (**Ceruti et al., 2006; Destanovic et al., 2018; Dittus et al., 2018; Lee et al., 2016; von Metzler et al., 2009**), which at first glance appeared to be at odds with our observation that proteasome inhibition enhances genome stability and survival of ETO-treated cells. We addressed this apparent discrepancy by showing that the timing of proteasome inhibition has a remarkable impact on the outcome of ETO treatment. Inhibiting proteasomal function prior to or during ETO administration significantly improved genome stability by minimizing DSB mis-repair associated with TOP2 proteolysis. However, inhibiting the proteasome after ETO treatment did not effectively protect cells from ETO-induced genome instability, presumably because proteasome-mediated degradation of TOP2ccs is an extremely fast process. Taken together, our study suggests that caution needs to be taken when scheduling therapeutic regimens combining topoisomerase poisons with proteasome inhibitors.

Our analysis also revealed that TOP2-mediated DSBs, especially ones that are not promptly repaired, undergo extensive DNA end-resection. We interpreted this as an indicator of active DNA repair occurring at TOP2ccs that have been partially or completely degraded by the proteasome. By contrast, when proteasomal degradation was inhibited by BTZ, we could only detect trace levels of DNA end-resection. This suggests the possibility that MRE11, which is required for DNA end-resection, may not recognize unprocessed TOP2. Similar to TOP2, the meiotic recombination initiator SPO11 forms protein-linked DSBs, which are thought to trigger MRE11 nuclease removal of SPO11 (**Neale et al., 2005**). However, recent studies reveal that mammalian meiotic cells accumulate significant levels of DNA-bound SPO11, which could, in principal be partially proteolyzed (**Paiano et al., 2020**). While the mechanism by which TOP2 (and perhaps SPO11) shields its associated DSB from early detection by DDR surveillance factors is unclear, our results highlight that γ -H2AX is only a reliable marker for proteolytically degraded TOP2ccs. In contrast, END-seq can be used to distinguish intact TOP2ccs, partially proteolyzed TOP2ccs, as well as fully processed protein-free DSBs.

Finally, we found that the SUMO-targeted ubiquitin ligase RNF4 played a critical role in recruiting the proteasome to degrade TOP2ccs, confirming a report by another group (**Sun et al., 2019**). The loss of RNF4 afforded cells significant protection from the genotoxic effects of ETO, further highlighting how impairing proteasome-mediated degradation of TOP2ccs can preserve genome integrity. However, RNF4 deletion did not prevent ETO-induced chromosomal aberrations or blunt the γ -H2AX response as efficiently as chemical proteasome inhibition. This indicates the likely existence of additional ubiquitin ligases that are functionally redundant to RNF4. Nevertheless, our data suggests that RNF4 could be potentially used as a biomarker to predict the effectiveness of chemotherapeutic regimens that incorporate topoisomerase poisons. In addition, de-regulation of RNF4 may represent a potential mechanism for tumors to acquire resistance to topoisomerase poisons by favoring TOP2cc reversal over degradation.

Materials and methods

Key resources table

Reagent type (Species or Source)	Designation	Source	Identifier	Add. info
Antibody	Anti-phospho-Histone H2A.X (Ser139) (mouse monoclonal)	Millipore	Cat# JBW301; RRID:AB_309864	(1:5000 - 1:10000)
Antibody	Anti-Tubulin (mouse monoclonal)	Sigma	Cat# T-5168 RRID:AB_477585	(1:5000)
Antibody	Anti-p53 (1CA2) (mouse monoclonal)	Cell Signaling	Cat# 2524 RRID:AB_331743	(1:2000)

Continued on next page

Continued

**Reagent type
(Species or
Source)**

Reagent type (Species or Source)	Designation	Source	Identifier	Add. info
Antibody	Anti-Vinculin (rabbit polyclonal)	Cell Signaling	Cat# 4650 RRID:AB_10559207	(1:2000)
Antibody	Anti-Top2b (rabbit polyclonal)	Novus	Cat# NB100-10842 RRID:AB_1522570	(1:5000)
Antibody	Anti-Rabbit Li-Cor (goat polyclonal)	Li-Cor	Cat# 926-32211; RRID:AB_621843	(1:10000)
Antibody	Anti-mouse IgG1 Alexa 488 (goat polyclonal)	Invitrogen	Cat# A-21121; RRID:AB_141514	(1:10000)
Antibody	Anti-H2AX (rabbit polyclonal)	Abcam	Cat# ab11175 RRID:AB_297814	(1:5000)
Chemical compound, Drug	Etoposide	Sigma	Cat# E1383	10–50 μ M
Chemical compound, Drug	Bortezomib	Millipore	Cat# 179324-69-7	1–5 μ M
Chemical compound, Drug	MG132	Sigma	Cat# 1211877-36-9	10 μ M
Chemical compound, Drug	Camptothecin	Sigma	Cat# 7689-03-4	12.5 μ M
Chemical compound, Drug	Ixaomib	Selleckchem	Cat# S2180	10 μ M
Chemical compound, Drug	Eponomicin	Sigma	Cat# 134381-21-8	2 μ M
Chemical compound, Drug	Doxycycline hyclate	Sigma	Cat# D9891	1 μ g/ml
Chemical compound, Drug	Imatinib mesylate (STI571)	Selleckchem	Cat# S1026	
Cell Line (<i>M. musculus</i>)	pre-B cell lines	Bredemeyer et al., 2006		
Cell Line (<i>M. musculus</i>)	RNF4 ^{-/-} MEFs	Generated by Gary Lyons, Hu et al., 2010		
Biological Sample (<i>M. musculus</i>)	Primary splenic B-cells		Freshly isolated from <i>M. musculus</i> spleen	
Strain (<i>M. musculus</i>)	C57BL/6NCr mice (WT)	Charles River	Strain code# 027	
Strain (<i>M. musculus</i>)	Conditional BRCA1- Δ 11f/f CD19-cre expressing mice	NCI mouse repository		
Strain (<i>M. musculus</i>)	H2AX ^{-/-} mice	Celeste et al., 2002		
Strain (<i>M. musculus</i>)	Conditional Lig4f/f expressing ERT2-Cre mice	Provided by P. Mckinnon		
Strain (<i>M. musculus</i>)	ATM ^{-/-} mice	Provided by A. Wynshaw-Boris		
Strain (<i>M. musculus</i>)	Conditional RNF4 f/f mice	Provided by S. Bunting		
Strain (<i>M. musculus</i>)	Conditional BRCA2 f/f CD19-cre expressing mice	Provided by S. Sharan		
Strain (<i>M. musculus</i>)	PolQ ^{-/-} mice	Provided by A. D'Andrea		
Recombinant DNA reagent	YFP ^u Degron reporter (plasmid)	Provided by A. Weissman Bence et al., 2005; Bence et al., 2001		(0.5 ng/ μ L)

Continued on next page

Continued

**Reagent type
(Species or
Source)****Designation****Source****Identifier****Add. info**

Peptide, recombinant protein	Lipopolysaccharide (LPS)	Sigma	Cat# L-2630	25 µg/ml
Peptide, recombinant protein	IL-4 from mouse, Interleukin-4, recombinant	Sigma	Cat# I-1020	5 ng/ml
Peptide, recombinant protein	RP105	BD Biosciences	Cat # 552128	0.5 µg/ml
Peptide, recombinant protein	Cy3-labeled (CCCTAA) peptide nucleic acid probe	PNA Bio	Cat# F1002	
Peptide, recombinant protein	Puregene Proteinase K solution	Qiagen	Cat# 19133	170 µL
Peptide, recombinant protein	Puregene RNaseA	Qiagen	Cat# 19101	50 µL
Peptide, recombinant protein	T4 DNA polymerase	NEB	Cat# M0203L	15 U
Peptide, recombinant protein	Klenow fragment	NEB	Cat# M0210M	5 U
Peptide, recombinant protein	T4 polynucleotide kinase	NEB	Cat# M0201L	15 U
Peptide, recombinant protein	Klenow exo-fragment	NEB	Cat# M0212M	15 U
Peptide, recombinant protein	Quick Ligase	NEB	Cat# M2200L	
Peptide, recombinant protein	USER enzyme	NEB	Cat# M5508L	
Peptide, recombinant protein	beta-agarase I	NEB	Cat# M0392S	1.5 µL
Commercial Assay Kit	CHEF Mammalian Genomic DNA plug kit	Bio-Rad	Cat# 1703591	
Commercial Assay Kit	Click-IT EdU Alexa Fluor 488 Flow Cytometry Assay Kit	ThermoFisher	Cat# C10425	
Commercial Assay Kit	KAPA Library Quantification Kit	Kapa Biosciences	Cat# KK4824	
Commercial Assay Kit	Celltiter-Glo Cell Viability Assay Kit	Promega	Cat# G7571	
Other	Streptavidin beads MyOne C1	ThermoFisher	Cat# 650-01	35 µL
Other	Anti-CD43 (Ly-48) MicroBeads (mouse)	Miltenyi Biotec	Cat# 130-049-80	
Other	Glycogen (20 mg/ml)	Roche	Cat# 10901393001	1 µL
Other	Kapa HiFi Hot Start Ready mix	Kapa Biosciences	Cat# KK2502	

Continued on next page

Continued

**Reagent type
(Species or
Source)**

Designation	Source	Identifier	Add. info
Other	Agencourt AM Pure XP beads	Beckman Coulter	Cat# A63881
Other	IrysPrep Lysis Buffer	BioNano Genomics	Cat# 20270
Other	X-tremeGene 9 Transfection Reagent	Sigma	Cat # XTG9-RO
Sequence-based reagent	END-seq hairpin adaptor 1, 5'-Phos-GATCGGAAGAGCGTCGTGTAGGGAAAGAGTGUU[Biotin-dT]U[Biotin-dT]UUACACTCTTCCCTACACGACGCTCTCCGATC*T-3'	Canela et al., 2016	END-seq sequence adapter
Sequence-based reagent	END-seq hairpin adaptor 2, 5'-Phos-GATCGGAAGAGCACACGTCTUUUUUUUUAGACGTGTGCTCTCCGATC*T-3'	Canela et al., 2016	END-seq sequence adapter
Sequence-based reagent	TruSeq barcoded primer p5, AATGATACGGCGACCACCGAGATCTACACNNNNNNNNNACACTCTTCCCTACACGACGCTCTCCGATC*T	Canela et al., 2019	END-seq sequence primer
Sequence-based reagent	TruSeq barcoded primer p7, CAAGCAGAAGACGGCATACGAGANNNNNNNNGTGACTGGAGTTCAGACGTGTGCTCTCCGATC*T	Canela et al., 2019	END-seq sequence primer
Software	Prism (7)	GraphPad	https://www.graphpad.com/scientific-software/prism/ RRID:SCR_002798
Software	Bowtie 1.1.2	Langmead et al., 2009	https://sourceforge.net/projects/bowtie-bio/files/bowtie/1.1.2/ RRID:SCR_005476
Software	MACS 1.4.3	Zhang et al., 2008	https://pypi.python.org/pypi/MACS/1.4.3
Software	UCSC database	Karolchik et al., 2004	https://genome.ucsc.edu RRID:SCR_005780
Software	UCSC Genome Browser	Kent et al., 2002	https://genome.ucsc.edu RRID:SCR_005780
Software	Bedtools	Quinlan and Hall, 2010	https://github.com/ark5x/bedtools2 RRID:SCR_006646
Software	Samtools	Li et al., 2009	https://github.com/samtools/samtools RRID:SCR_002105
Software	Knight-Ruiz algorithm	Rao et al., 2014	https://academic.oup.com/imajna/article-lookup/DOI:10.1093/imanum/drs019
Software	R	R Development Core Team (2008)	https://www.r-project.org/ RRID:SCR_001905
Software	FlowJo (10.1)	FlowJo LLC	https://www.flowjo.com/ RRID:SCR_008520
Software	Metapher ISIS	Metapher Systems	
Software	hiSKY 7.2.7	ADS Biotech	

Mice

C57BL/6 WT (NCI mouse repository), POLQ^{-/-} (provided by A. D'Andrea), H2AX^{-/-} (**Celeste et al., 2002**), ATM^{-/-} (provided by A. Wynshaw-Boris) and conditional Lig4^{-/-} (Lig4^{f/f;ERT2-Cre}, provided by P. McKinnon), BRCA1^{Δ11}BRCA1^{f/f;CD19Cre}, **Zong et al. (2019)**, BRCA2^{-/-} (BRCA2^{f/f;CD19Cre}, provided by

S. Sharan) and RNF4^{-/-} (RNF4^{f/f;CD19Cre}) mice between 8 and 18 weeks of age were used to prepare single cell suspensions of primary splenic B-cells. All animal experiments were approved by the NCI Animal Care and Use Committee (Protocol Numbers: EIB-064–3 and 17–042).

Cell culture methods

Mature resting B-cells were isolated from mouse spleen with anti-CD43 MicroBeads (Miltenyi Biotech). B-cells were activated with LPS (25 µg/ml; Sigma), IL-4 (5 ng/ml; Sigma-Aldrich) and RP105 (0.5 µg/ml; BD Biosciences) for 12 hr as described (Barlow et al., 2013; Callén et al., 2007). Lymphocyte separation media (Corning) was used after harvesting the B-cells to separate dead cells from live cells prior to use for END-seq protocol. Cellular Viability was measured using CellTiter-Glo Cell Viability Assay Kit (Promega) according to manufactures directions. Luminescence was quantified using a Tecan Infinite M200 Pro plate reader. B-cells were pre-treated with proteasome inhibitor, either 10 µM MG132 (Sigma-Aldrich) or 5 µM Bortezomib (Millipore) for 1 hr then co-treated for an additional 2 hr with 50 µM Etoposide (E1383, Sigma-Aldrich). Following the ETO pulse, the cells were either harvested in the presence of the drugs, or washed three times in ice-cold drug free media (3 × 5 min spin at 1500 rpm and 4°C to pellet B-cells between washes; 15–20 min total time to complete washout), and returned to 37°C to recover in fresh drug free media, until they were harvested at various timepoints post-washout for END-seq, western blot, Immunofluorescence, ICE assay, or for mitotic spread analysis as described in Figure 1A. Asynchronous WT B-cells were treated 24 hr post-activation for 2 hr with 50 µM ETO or 12.5 µM Camptothecin (Sigma-Aldrich) ±1 hr 10 µM MG132 pre-treatment, then fixed following a 24 hr recovery in drug free media for mitotic spread analysis. Abelson-transformed pre-B cells (Bredemeyer et al., 2006) were retrovirally transduced with the tetracycline-inducible ER-AsiSI, pTRE3G-HA-ER-AsiSI as previously described (Callen et al., 2013). WT and RNF4^{-/-} MEFs (generated by Gary Lyons) (Hu et al., 2010) were cultured in DMEM (Invitrogen) + 10% FBS and 1% PenStrep (Invitrogen). MEFs were treated with 5–20 µM ETO for 1 hr ±1 µM BTZ 1 hr pretreatment. For END-seq experiments that used Zinc Finger Nuclease (ZFN) spike-in normalization, induction of ZFN was done in G1-arrested Lig4^{-/-} pre B cells (Bredemeyer et al., 2006) by treating with imatinib for 48 hr and 1 µg/ml Doxycycline during the last 24 hr as described (Canela et al., 2016; Bredemeyer et al., 2006).

WT and Lig4^{-/-} mouse pre B cell lines were provided by B. Sleckman. WT and RNF4^{-/-} mouse embryonic fibroblasts (MEFs) were provided by S. Bunting. These cell lines are negative for mycoplasma.

γ-H2AX and pan-p53 western blot

Western blotting for γ-H2AX and pan-p53 was performed using γ-H2AX antibody (Millipore) at 1:5000 dilution and p53 antibody (Cell Signaling) at 1:2000 dilution. Antibodies recognizing tubulin (Sigma-Aldrich, 1:5000), H2AX (Millipore, 1:5000) and vinculin (Cell Signaling, 1:2000) were used to control for protein loading. Image analysis was done using Li-Cor Odyssey CLx to quantify band intensity.

In vitro of complex (ICE) Assay

Topoisomerase II DNA-protein complexes (TOP2-DPCs) were isolated and detected using in vivo complex of enzyme (ICE) assay as previously described (Anand et al., 2018). Briefly, 5 million cells were lysed in sarkosyl solution (1% w/v) after treatment. Cell lysates were sheared through a 25 g 5/8 needle (10 strokes) to reduce the viscosity of DNA and layered onto CsCl solution (150% w/v), followed by centrifugation in NVT 65.2 rotor (Beckman coulter) at 42,000 RPM for 20 hr at 25°C. The resulting pellet containing nucleic acids and TOP2-DPCs was obtained and dissolved in TE buffer. The samples were subjected to immunoblotting (slot blot) with anti-mouse TOP2β antibody (Novus). 2 µg of DNA is applied per sample. TOP2-DPCs were quantified by densitometric analysis using ImageJ.

Metaphase spread, FISH and SKY analysis

5 million cells were harvested 24 hr after drugs were washed out for metaphase analysis as described (Callén et al., 2007). Quantitative FISH analysis using a Cy3-labeled (CCCTAA) peptide nucleic acid probe (Applied Biosystems) was performed as described previously (Callén et al., 2007). Telomere

length measurements were performed on at least 15 metaphases for each cell type. DAPI chromosome and Cy3 telomere images were acquired with a constant exposure time that ensured all captured fluorescent signals were within the linear range using Metafer Software on a Zeiss Axio Imager Z2 Microscope. Image analysis was done in the Metafer ISIS software. SKY was performed and analyzed as previously described, using the hiSKY 7.2.7 Software (ASI) on a Leica DMRXA Microscope (Liyana *et al.*, 1996). A minimum of 35 metaphases were imaged and analyzed.

YFP^udegron quantification

WT eHAP cells were transfected for 48 hr using Xtreme Gene 9 transfection reagent with YFP^u Degron reporter (0.5 ng/μL) as described (Bence *et al.*, 2005; Bence *et al.*, 2001). eHAP cells were then treated 48 hr post-transfection with 1 μM BTZ and 5 μM MG132 for 2 hr to mimic the total amount of time the proteasome inhibitors are incubated in primary B-cells, after which the cells were washed three times and left to recover at 37°C for up to 18 hr. Cells were fixed at 2 hr, 6 hr, and 18 hr after washout with 4% PFA and YFP expression was measured on a FACS Cantoll (BD biosciences).

EdU staining

To measure DNA synthesis, primary B-cell cultures were stimulated for 12 hr, 24 hr, 28 hr or 36 hr pulsed with 10 μM of EdU (5-ethynyl-2'-deoxyuridine) for 30 min at 37°C and stained using the Click-IT EdU Alexa Fluor 488 Flow Cytometry Assay Kit according to the manufacturer's specifications (Thermo Fisher C10425). Samples were acquired on a FACS Cantoll (BD biosciences).

Immunofluorescence

Immunofluorescence staining with γ-H2AX antibody (Millipore, 1:10,000) was performed in parallel in WT pre B cells (Bredemeyer *et al.*, 2006) to verify DSB induction.

END-seq

Single cell suspensions of primary B-cells (15–20 million) were untreated or treated with drugs to inhibit the proteasome and/or etoposide as indicated in the cell culture methods section. Primary B-cells were washed twice in cold PBS and resuspended in cold cell suspension buffer (Bio-Rad CHEF Mammalian Genomic DNA plug kit), equilibrated for 5 min at room temperature, mixed with 2% melted CleanCut agarose (Bio-Rad CHEF Mammalian Genomic DNA plug kit) prewarmed at 37°C for a final concentration of 0.75%, and transferred immediately into plug molds and let them solidify at 4°C for 20 min. Embedded cells were lysed and digested using Proteinase K (50°C, 1 hr then 37°C for 7 hr). Etoposide and drugs were maintained at the same experimental concentrations in all the steps until digestion with Proteinase K. Plugs were rinsed in TE buffer and treated with RNaseA at 37°C, 1 hr. The next enzymatic reactions were performed with the DNA in agarose plugs to prevent shearing. DNA ends were blunted for 1 hr at 37°C with Exonuclease VII (ExoVII) followed by Exonuclease T (ExoT) (NEB) for 1 hr at 25°C to detect all TOP2-mediated DSBs (protein-linked and protein-free), or only with Exonuclease T (NEB) for 1 hr at 25°C to detect only protein-free DSBs. After blunting, A-tailing was performed to attach dA to the free 3'-OH, followed by ligation of "END-seq hairpin adaptor 1," listed in reagents section, using NEB Quick Ligase. Agarose plugs were then melted and dialyzed, and DNA was sonicated to a median shear length of 170 bp using Covaris S220 sonicator for 4 min at 10% duty cycle, peak incident power 175, 200 cycles per burst, at 4°C. DNA was ethanol-precipitated and dissolved in 70 ml TE buffer. Biotinylated DNA was isolated using MyOne Streptavidin C1 Beads (Thermo Fisher #650-01), followed by end repair (dNTPs, T4 polymerase (NEB), Klenow (NEB), T4 PNK) and dA-tailing (Klenow exo- (NEB), dATP). The second end was ligated to "END-seq hairpin adaptor 2" using NEB Quick Ligase. Hairpins were digested using USER (NEB), and the resulting DNA fragments were PCR amplified using TruSeq barcoded primer p5, AATGATACGGCGACCACCGAGATCTACACNNNNNNNNNACACTCTTCCCTACACGACGCTCTCCGATC*T and TruSeq barcoded primer p7, CAAGCAGAAGACGGCATACGAGANNNNNNNGTGACTGGAGTTCAGACGTGTGCTCTTCCGATC*T, (NNNNNNNNN represents barcode a * a phosphothiorate bond) listed in reagents. PCR fragments were isolated by size selection from agarose gel, selecting 200–500 bp fragments followed by DNA purification using QIAquick Gel Extraction Kit. Libraries were quantified using KAPA Library Quantification Kit and sequenced using

Illumina NextSeq 500 or 550. A detailed END-seq protocol can be found in *Canela et al. (2017)*, as well as more information about the ExoVII and ExoT processing of TOP2-mediated DSBs in *Canela et al. (2019)*.

Quantification and statistical analysis

Genome alignment

END-seq single end reads were aligned to the mouse genome (GRCm38p2/mm10) using Bowtie v1.1.2 (*Langmead and Salzberg, 2012*) with parameters (-n 3 k 1 l 50) and alignment files were generated and sorted using SAMtools (*Li et al., 2009*) and BEDtools (*Quinlan and Hall, 2010*).

Peak calling

Peaks were called using MACS 1.4.3 (*Zhang et al., 2008*) with the parameters: -nolambda,-nomodel and-keep-dup = all (keep all redundant reads). For ETO-treated END-seq data peak calling, we used the corresponding non-treated samples as control, keeping >10 fold-enriched peaks. The peaks within blacklisted regions (<https://sites.google.com/site/anshulkundaje/projects/blacklists>) were filtered. For primary B-cell data, in order to perform a direct comparison of the breaks across experiments, peak calling was done on the END-seq (ExoT+ExoVII) data presented in *Figure 2* (carried out after 2 hr of ETO) and in *Figure 2—figure supplement 1*. As the END-seq signal is very reproducible between replicates (*Figure 2—figure supplement 1*), all of the analyses thereafter including persistence, reversibility and resection presented in *Figures 2* and *3*, utilized the peak dataset from replicate 1. Analysis using the peak dataset from replicate two is presented in *Figure 2—figure supplement 1* and *Figure 3—figure supplement 1*.

END-seq data analysis

For comparisons between different genotypes and treatments, END-seq signal was calculated, as RPKM, within END-seq peaks, for the corresponding cell type. For END-seq data, all reads were counted. For END-seq data, where cells with ZFN break were spiked-in to the library at a 1:40 (2.5%) ratio, the RPKM value for each peak was divided by the signal around the spiked-in breaks and then multiplied by 2.5, to get values as cell-percentage.

Resection quantification

To quantify the width of maximum resection endpoint, a sliding window containing 10 50 bp bins was used to start from the summit of each break, out to 2.5 kb on either side of the summit to detect the END-seq signal around the break summit. Maximum END-seq signal for 50 bp bins within 2.5 kb -5 kb around break summit was used as background. When more than half of the bins within this sliding window had an RPKM values equal to or lower than the background, then the last bin within the window which had a detectable signal over background is regarded as the maximum resection endpoint from the break summit. Only breaks having >100 bp resection signal were considered for the comparison of resection length in *Figure 3*.

Classification of TOP2-mediated DSBs

The fraction of the different TOP2-mediated DSB species (Reversible TOP2cc, Irreversible TOP2cc and protein-free DSB) were calculated as follows: First, ExoT END-seq signal was divided by the END-seq signal (using ExoVII+ExoT) for all TOP2-mediated DSB sites (determined by peak calling as described above), to obtain the protein-free DSB fraction ([DSB]) (*Chase and Richardson, 1974*). Similarly, TOP2cc fraction, [TOP2CC], was defined as [TOP2CC]=1-[DSB] fraction for each lesion. To calculate the reversible TOP2cc fraction ([TOP2CC]_R), we subtracted the data obtained from the END-seq ETO washout experiment (see above), from the data obtained from END-seq ETO experiment without washout, to get [TOP2CC]_R. Finally, the irreversible TOP2cc fraction ([TOP2CC]_I) was defined as [TOP2CC]_I = 1-[DSB]-[TOP2CC]_R. A more detailed description of this analysis can be found in *Canela et al. (2019)*.

Data visualization

Aligned-reads bed files were first converted to bedgraph files using bedtools genomcov (*Quinlan and Hall, 2010*) following by bedGraphToBigWig to make a bigwig file (*Kent et al., 2002*).

Visualization of genomic profiles was done by the UCSC browser (*Kent et al., 2002*). Genome browser profiles were normalized to the library size (RPM) and spike-in.

Statistical analysis

Statistical analysis was performed using R version 3.5.0 (<http://www.r-project.org>). The statistical tests are reported in the figure legend and main text.

Acknowledgements

We thank Keith Caldecott for comments on the manuscript, Allan Weissman for providing the YFP^u Degron, Rachel Burga for support with statistical analysis and generating the graphic schematic and Jennifer Wise and Kelly Smith for assistance with animal work. The AN laboratory is supported by the Intramural Research Program of the NIH, a Department of Defense awards W81XWH-16-1-599 and W81XWH-19-1-0712 and an NIH Intramural FLEX Award.

Additional information

Funding

Funder	Grant reference number	Author
National Institutes of Health	Intramural Research Program	André Nussenzweig
Ellison Medical Foundation	Senior Scholar in Aging Award AG-SS- 2633-11	André Nussenzweig
U.S. Department of Defense	Idea Expansion Award W81XWH-15-2-006	André Nussenzweig
U.S. Department of Defense	Idea Breakthrough Award W81XWH-16-1-599	André Nussenzweig
Alex's Lemonade Stand Foundation		André Nussenzweig
National Institutes of Health	Intramural FLEX Award	André Nussenzweig


The funders had no role in study design, data collection and interpretation, or the decision to submit the work for publication.

Author contributions

Nicholas Sciascia, Conceptualization, Data curation, Software, Formal analysis, Validation, Investigation, Visualization, Methodology, Project administration; Wei Wu, Data curation, Software, Formal analysis, Visualization, Methodology; Dali Zong, Formal analysis, Investigation, Methodology, Writing - original draft, Writing - review and editing; Yilun Sun, Formal analysis, Investigation, Visualization; Nancy Wong, Investigation; Sam John, Writing - original draft, Writing - review and editing; Darawalee Wangsa, Data curation, Formal analysis, Investigation, Visualization; Thomas Ried, Formal analysis, Methodology; Samuel F Bunting, Resources, Provided the RNF4 conditional knockout mice; Yves Pommier, Conceptualization, Methodology; André Nussenzweig, Conceptualization, Resources, Supervision, Funding acquisition, Validation, Methodology, Writing - original draft, Project administration, Writing - review and editing

Author ORCIDs

Nicholas Sciascia  <https://orcid.org/0000-0003-4169-4929>

André Nussenzweig  <https://orcid.org/0000-0002-8952-7268>

Ethics

Animal experimentation: All mouse breeding and experimentation followed protocols approved by the National Institutes of Health Institutional Animal Care and Use Committee (Protocol Numbers: EIB-064-3 and 17-042).

Decision letter and Author responseDecision letter <https://doi.org/10.7554/eLife.53447.sa1>Author response <https://doi.org/10.7554/eLife.53447.sa2>**Additional files****Supplementary files**

- Supplementary file 1. Table of experimental replicates for each figure panel.
- Transparent reporting form

Data availability

Sequencing data has been deposited in GEO under the accession code GSE140372.

The following dataset was generated:

Author(s)	Year	Dataset title	Dataset URL	Database and Identifier
Sciascia N, Wu W, Zong D, Sun Y, Wong N, Wangsa D, John S, Ried T, Bunting S, Pommier Y, Nussenzweig A	2019	Suppressing Proteasome Mediated Processing of Topoisomerase II DNA-Protein Adducts Preserves Genome Integrity	https://www.ncbi.nlm.nih.gov/geo/query/acc.cgi?acc=GSE140372	NCBI Gene Expression Omnibus, GSE140372

References

- An WG, Hwang SG, Trepel JB, Blagosklonny MV. 2000. Protease inhibitor-induced apoptosis: accumulation of wt p53, p21WAF1/CIP1, and induction of apoptosis are independent markers of proteasome inhibition. *Leukemia* **14**:1276–1283. DOI: <https://doi.org/10.1038/sj.leu.2401812>, PMID: 10914553
- Anand J, Sun Y, Zhao Y, Nitiss KC, Nitiss JL. 2018. Detection of topoisomerase covalent complexes in eukaryotic cells. *Methods in Molecular Biology* **1703**:283–299. DOI: https://doi.org/10.1007/978-1-4939-7459-7_20, PMID: 29177749
- Aras B, Yerlikaya A. 2016. Bortezomib and etoposide combinations exert synergistic effects on the human prostate Cancer cell line PC-3. *Oncology Letters* **11**:3179–3184. DOI: <https://doi.org/10.3892/ol.2016.4340>, PMID: 27123085
- Baranello L, Kouzine F, Wojtowicz D, Cui K, Przytycka TM, Zhao K, Levens D. 2014. DNA break mapping reveals topoisomerase II activity genome-wide. *International Journal of Molecular Sciences* **15**:13111–13122. DOI: <https://doi.org/10.3390/ijms150713111>, PMID: 25056547
- Barlow JH, Faryabi RB, Callén E, Wong N, Malhowski A, Chen HT, Gutierrez-Cruz G, Sun HW, McKinnon P, Wright G, Casellas R, Robbiani DF, Staudt L, Fernandez-Capetillo O, Nussenzweig A. 2013. Identification of early replicating fragile sites that contribute to genome instability. *Cell* **152**:620–632. DOI: <https://doi.org/10.1016/j.cell.2013.01.006>, PMID: 23352430
- Bence NF, Sampat RM, Kopito RR. 2001. Impairment of the ubiquitin-proteasome system by protein aggregation. *Science* **292**:1552–1555. DOI: <https://doi.org/10.1126/science.292.5521.1552>, PMID: 11375494
- Bence NF, Bennett EJ, Kopito RR. 2005. Application and Analysis of the GFPu Family of Ubiquitin-Proteasome System Reporters. In: *Methods in Enzymology*. Academic Press. p. 481–490. DOI: [https://doi.org/10.1016/S0076-6879\(05\)99033-2](https://doi.org/10.1016/S0076-6879(05)99033-2)
- Bredemeyer AL, Sharma GG, Huang CY, Helmink BA, Walker LM, Khor KC, Nuskey B, Sullivan KE, Pandita TK, Bassing CH, Sleckman BP. 2006. ATM stabilizes DNA double-strand-break complexes during V(D)J recombination. *Nature* **442**:466–470. DOI: <https://doi.org/10.1038/nature04866>, PMID: 16799570
- Callén E, Jankovic M, Difilippantonio S, Daniel JA, Chen HT, Celeste A, Pellegrini M, McBride K, Wangsa D, Bredemeyer AL, Sleckman BP, Ried T, Nussenzweig M, Nussenzweig A. 2007. ATM prevents the persistence and propagation of chromosome breaks in lymphocytes. *Cell* **130**:63–75. DOI: <https://doi.org/10.1016/j.cell.2007.06.016>, PMID: 17599403
- Callen E, Di Virgilio M, Kruhlak MJ, Nieto-Soler M, Wong N, Chen HT, Faryabi RB, Polato F, Santos M, Starnes LM, Wesemann DR, Lee JE, Tubbs A, Sleckman BP, Daniel JA, Ge K, Alt FW, Fernandez-Capetillo O, Nussenzweig MC, Nussenzweig A. 2013. 53bp1 mediates productive and mutagenic DNA repair through distinct phosphoprotein interactions. *Cell* **153**:1266–1280. DOI: <https://doi.org/10.1016/j.cell.2013.05.023>, PMID: 23727112
- Canela A, Sridharan S, Sciascia N, Tubbs A, Meltzer P, Sleckman BP, Nussenzweig A. 2016. DNA Breaks and End Resection Measured Genome-wide by End Sequencing. *Molecular Cell* **63**:898–911. DOI: <https://doi.org/10.1016/j.molcel.2016.06.034>

- Canela A**, Maman Y, Jung S, Wong N, Callen E, Day A, Kieffer-Kwon K-R, Pekowska A, Zhang H, Rao SSP, Huang S-C, Mckinnon PJ, Aplan PD, Pommier Y, Aiden EL, Casellas R, Nussenzweig A. 2017. Genome organization drives chromosome fragility. *Cell* **170**:507–521. DOI: <https://doi.org/10.1016/j.cell.2017.06.034>
- Canela A**, Maman Y, Huang SN, Wutz G, Tang W, Zagnoli-Vieira G, Callen E, Wong N, Day A, Peters JM, Caldecott KW, Pommier Y, Nussenzweig A. 2019. Topoisomerase II-Induced chromosome breakage and translocation is determined by chromosome architecture and transcriptional activity. *Molecular Cell* **75**:252–266. DOI: <https://doi.org/10.1016/j.molcel.2019.04.030>, PMID: 31202577
- Celeste A**, Petersen S, Romanienko PJ, Fernandez-Capetillo O, Chen HT, Sedelnikova OA, Reina-San-Martin B, Coppola V, Meffre E, Difilippantonio MJ, Redon C, Pilch DR, Oлару A, Eckhaus M, Camerini-Otero RD, Tessarollo L, Livak F, Manova K, Bonner WM, Nussenzweig MC, et al. 2002. Genomic instability in mice lacking histone H2AX. *Science* **296**:922–927. DOI: <https://doi.org/10.1126/science.1069398>, PMID: 11934988
- Ceruti S**, Mazzola A, Abbraccio MP. 2006. Proteasome inhibitors potentiate etoposide-induced cell death in human astrocytoma cells bearing a mutated p53 isoform. *Journal of Pharmacology and Experimental Therapeutics* **319**:1424–1434. DOI: <https://doi.org/10.1124/jpet.106.109397>, PMID: 16971507
- Chase JW**, Richardson CC. 1974. Exonuclease VII of *Escherichia coli*. Mechanism of action. *The Journal of Biological Chemistry* **249**:4553–4561. PMID: 4602030
- Cowell IG**, Austin CA. 2012. Mechanism of generation of therapy related leukemia in response to anti-topoisomerase II agents. *International Journal of Environmental Research and Public Health* **9**:2075–2091. DOI: <https://doi.org/10.3390/ijerph9062075>, PMID: 22829791
- Destanovic E**, Boos J, Lanvers-Kaminsky C. 2018. Preclinical evaluation of combined topoisomerase and proteasome inhibition against pediatric malignancies. *Anticancer Research* **38**:3977–3984. DOI: <https://doi.org/10.21873/anticancer.12684>, PMID: 29970520
- Dittus C**, Grover N, Ellsworth S, Tan X, Park SI. 2018. Bortezomib in combination with dose-adjusted EPOCH (etoposide, prednisone, vincristine, cyclophosphamide, and doxorubicin) induces long-term survival in patients with plasmablastic lymphoma: a retrospective analysis. *Leukemia & Lymphoma* **59**:2121–2127. DOI: <https://doi.org/10.1080/10428194.2017.1416365>, PMID: 29303024
- Errington F**, Willmore E, Leontiou C, Tilby MJ, Austin CA. 2004. Differences in the longevity of topo iia and topo iib drug-stabilized cleavable complexes and the relationship to drug sensitivity. *Cancer Chemotherapy and Pharmacology* **53**:155–162. DOI: <https://doi.org/10.1007/s00280-003-0701-1>, PMID: 14504921
- Gittens WH**, Johnson DJ, Allison RM, Cooper TJ, Thomas H, Neale MJ. 2019. A nucleotide resolution map of Top2-linked DNA breaks in the yeast and human genome. *Nature Communications* **10**:4846. DOI: <https://doi.org/10.1038/s41467-019-12802-5>
- Gómez-Herreros F**, Romero-Granados R, Zeng Z, Alvarez-Quilón A, Quintero C, Ju L, Umans L, Vermeire L, Huylebroeck D, Caldecott KW, Cortés-Ledesma F. 2013. TDP2-dependent non-homologous end-joining protects against topoisomerase II-induced DNA breaks and genome instability in cells and in vivo. *PLOS Genetics* **9**:e1003226. DOI: <https://doi.org/10.1371/journal.pgen.1003226>, PMID: 23505375
- Gómez-Herreros F**, Zagnoli-Vieira G, Ntai I, Martínez-Macías MI, Anderson RM, Herrero-Ruiz A, Caldecott KW. 2017. TDP2 suppresses chromosomal translocations induced by DNA topoisomerase II during gene transcription. *Nature Communications* **8**:1–9. DOI: <https://doi.org/10.1038/s41467-017-00307-y>
- Halasi M**, Pandit B, Gartel AL. 2014. Proteasome inhibitors suppress the protein expression of mutant p53. *Cell Cycle* **13**:3202–3206. DOI: <https://doi.org/10.4161/15384101.2014.950132>, PMID: 25485499
- Hoa NN**, Shimizu T, Zhou ZW, Wang ZQ, Deshpande RA, Paull TT, Akter S, Tsuda M, Furuta R, Tsutsui K, Takeda S, Sasanuma H. 2016. Mre11 is essential for the removal of lethal topoisomerase 2 covalent cleavage complexes. *Molecular Cell* **64**:580–592. DOI: <https://doi.org/10.1016/j.molcel.2016.10.011>, PMID: 27814490
- Hsiang YH**, Liu LF. 1989. Evidence for the reversibility of cellular DNA lesion induced by mammalian topoisomerase II poisons. *The Journal of Biological Chemistry* **264**:9713–9715. PMID: 2542330
- Hu XV**, Rodrigues TM, Tao H, Baker RK, Miraglia L, Orth AP, Lyons GE, Schultz PG, Wu X. 2010. Identification of RING finger protein 4 (RNF4) as a modulator of DNA demethylation through a functional genomics screen. *PNAS* **107**:15087–15092. DOI: <https://doi.org/10.1073/pnas.1009025107>, PMID: 20696907
- Karolchik D**, Hinrichs AS, Furey TS, Roskin KM, Sugnet CW, Haussler D, Kent WJ. 2004. The UCSC table browser data retrieval tool. *Nucleic Acids Research* **32**:493D–496. DOI: <https://doi.org/10.1093/nar/gkh103>, PMID: 14681465
- Kent WJ**, Sugnet CW, Furey TS, Roskin KM, Pringle TH, Zahler AM, Haussler D. 2002. The human genome browser at UCSC. *Genome Research* **12**:996–1006. DOI: <https://doi.org/10.1101/gr.229102>, PMID: 12045153
- Kisselev AF**, Goldberg AL. 2001. Proteasome inhibitors: from research tools to drug candidates. *Chemistry & Biology* **8**:739–758. DOI: [https://doi.org/10.1016/S1074-5521\(01\)00056-4](https://doi.org/10.1016/S1074-5521(01)00056-4)
- Langmead B**, Trapnell C, Pop M, Salzberg SL. 2009. Ultrafast and memory-efficient alignment of short DNA sequences to the human genome. *Genome Biology* **10**:R25. DOI: <https://doi.org/10.1186/gb-2009-10-3-r25>, PMID: 19261174
- Langmead B**, Salzberg SL. 2012. Fast gapped-read alignment with bowtie 2. *Nature Methods* **9**:357–359. DOI: <https://doi.org/10.1038/nmeth.1923>, PMID: 22388286
- Ledesma FC**, El Khamisy SF, Zuma MC, Osborn K, Caldecott KW. 2009. A human 5'-tyrosyl DNA phosphodiesterase that repairs topoisomerase-mediated DNA damage. *Nature* **461**:674–678. DOI: <https://doi.org/10.1038/nature08444>
- Lee KC**, Padget K, Curtis H, Cowell IG, Moiani D, Sondka Z, Morris NJ, Jackson GH, Cockell SJ, Tainer JA, Austin CA. 2012. MRE11 facilitates the removal of human topoisomerase II complexes from genomic DNA. *Biology Open* **1**:863–873. DOI: <https://doi.org/10.1242/bio.20121834>, PMID: 23213480

- Lee KC, Bramley RL, Cowell IG, Jackson GH, Austin CA. 2016. Proteasomal inhibition potentiates drugs targeting DNA topoisomerase II. *Biochemical Pharmacology* **103**:29–39. DOI: <https://doi.org/10.1016/j.bcp.2015.12.015>
- Lee K, Swan R, Sondka Z, Padget K, Cowell I, Austin C. 2018. Effect of TDP2 on the level of TOP2-DNA complexes and SUMOylated TOP2-DNA complexes. *International Journal of Molecular Sciences* **19**:2056. DOI: <https://doi.org/10.3390/ijms19072056>
- Li H, Handsaker B, Wysoker A, Fennell T, Ruan J, Homer N, Marth G, Abecasis G, Durbin R, 1000 Genome Project Data Processing Subgroup. 2009. The sequence alignment/Map format and SAMtools. *Bioinformatics* **25**:2078–2079. DOI: <https://doi.org/10.1093/bioinformatics/btp352>, PMID: 19505943
- Lin CP, Ban Y, Lyu YL, Desai SD, Liu LF. 2008. A ubiquitin-proteasome pathway for the repair of topoisomerase I-DNA covalent complexes. *Journal of Biological Chemistry* **283**:21074–21083. DOI: <https://doi.org/10.1074/jbc.M803493200>, PMID: 18515798
- Liyanaige M, Coleman A, du Manoir S, Veldman T, McCormack S, Dickson RB, Barlow C, Wynshaw-Boris A, Janz S, Wienberg J, Ferguson-Smith MA, Schröck E, Ried T. 1996. Multicolour spectral karyotyping of mouse chromosomes. *Nature Genetics* **14**:312–315. DOI: <https://doi.org/10.1038/ng1196-312>, PMID: 8896561
- Long BH, Musial ST, Brattain MG. 1985. Single- and double-strand DNA breakage and repair in human lung adenocarcinoma cells exposed to etoposide and teniposide. *Cancer Research* **45**:3106–3112. PMID: 3839166
- Manasanch EE, Orlowski RZ. 2017. Proteasome inhibitors in cancer therapy. *Nature Reviews Clinical Oncology* **14**:417–433. DOI: <https://doi.org/10.1038/nrclinonc.2016.206>
- Mao Y, Desai SD, Ting CY, Hwang J, Liu LF. 2001. 26 S proteasome-mediated degradation of topoisomerase II cleavable complexes. *Journal of Biological Chemistry* **276**:40652–40658. DOI: <https://doi.org/10.1074/jbc.M104009200>, PMID: 11546768
- Mårtensson S, Nygren J, Osheroff N, Hammarsten O. 2003. Activation of the DNA-dependent protein kinase by drug-induced and radiation-induced DNA strand breaks. *Radiation Research* **160**:291–301. DOI: [https://doi.org/10.1667/0033-7587\(2003\)160\[0291:AOTDPK\]2.0.CO;2](https://doi.org/10.1667/0033-7587(2003)160[0291:AOTDPK]2.0.CO;2), PMID: 12926987
- Muslimović A, Nyström S, Gao Y, Hammarsten O. 2009. Numerical analysis of etoposide induced DNA breaks. *PLOS ONE* **4**:e5859. DOI: <https://doi.org/10.1371/journal.pone.0005859>, PMID: 19516899
- Neale MJ, Pan J, Keeney S. 2005. Endonucleolytic processing of covalent protein-linked DNA double-strand breaks. *Nature* **436**:1053–1057. DOI: <https://doi.org/10.1038/nature03872>, PMID: 16107854
- Nitiss JL. 2009a. DNA topoisomerase II and its growing repertoire of biological functions. *Nature Reviews Cancer* **9**:327–337. DOI: <https://doi.org/10.1038/nrc2608>, PMID: 19377505
- Nitiss JL. 2009b. Targeting DNA topoisomerase II in Cancer chemotherapy. *Nature Reviews Cancer* **9**:338–350. DOI: <https://doi.org/10.1038/nrc2607>, PMID: 19377506
- Paiano J, Wu W, Yamada S, Sciascia N, Callen E, Paola Cotrim A, Deshpande RA, Maman Y, Day A, Paull TT, Nussenzweig A. 2020. ATM and PRDM9 regulate SPO11-bound recombination intermediates during meiosis. *Nature Communications* **11**:857. DOI: <https://doi.org/10.1038/s41467-020-14654-w>, PMID: 32051414
- Palumbo A, Gay F, Brinchen S, Falcone A, Pescosta N, Callea V, Caravita T, Morabito F, Magarotto V, Ruggeri M, Avonto I, Musto P, Cascavilla N, Bruno B, Boccadoro M. 2008. Bortezomib, doxorubicin and dexamethasone in advanced multiple myeloma. *Annals of Oncology* **19**:1160–1165. DOI: <https://doi.org/10.1093/annonc/mdn018>, PMID: 18326520
- Pommier Y, Sun Y, Huang S-yinN, Nitiss JL. 2016. Roles of eukaryotic topoisomerases in transcription, replication and genomic stability. *Nature Reviews Molecular Cell Biology* **17**:703–721. DOI: <https://doi.org/10.1038/nrm.2016.111>
- Quinlan AR, Hall IM. 2010. BEDTools: a flexible suite of utilities for comparing genomic features. *Bioinformatics* **26**:841–842. DOI: <https://doi.org/10.1093/bioinformatics/btq033>, PMID: 20110278
- R Development Core Team. 2008. R: A language and environment for statistical computing. *R Foundation for Statistical Computing*. Vienna, Austria, <http://www.R-project.org/>
- Rao SS, Huntley MH, Durand NC, Stamenova EK, Bochkov ID, Robinson JT, Sanborn AL, Machol I, Omer AD, Lander ES, Aiden EL. 2014. A 3D map of the human genome at Kilobase resolution reveals principles of chromatin looping. *Cell* **159**:1665–1680. DOI: <https://doi.org/10.1016/j.cell.2014.11.021>, PMID: 25497547
- Rastogi N, Mishra DP. 2012. Therapeutic targeting of Cancer cell cycle using proteasome inhibitors. *Cell Division* **7**:26. DOI: <https://doi.org/10.1186/1747-1028-7-26>, PMID: 23268747
- Schellenberg MJ, Lieberman JA, Herrero-Ruiz A, Butler LR, Williams JG, Muñoz-Cabello AM, Mueller GA, London RE, Cortés-Ledesma F, Williams RS. 2017. ZATT (ZNF451)-mediated resolution of topoisomerase 2 DNA-protein cross-links. *Science* **357**:1412–1416. DOI: <https://doi.org/10.1126/science.aam6468>, PMID: 28912134
- Sun Y, Jenkins LMM, Su YP, Nitiss KC, Nitiss JL, Pommier Y. 2019. A conserved SUMO-Ubiquitin pathway directed by RNF4/SLX5-SLX8 and PIAS4/SIZ1 drives proteasomal degradation of topoisomerase DNA-protein crosslinks. *bioRxiv*. DOI: <https://doi.org/10.1101/707661>
- Sunter NJ, Cowell IG, Willmore E, Watters GP, Austin CA. 2010. Role of topoisomerase $\text{ii}\beta$ in DNA damage response following IR and etoposide. *Journal of Nucleic Acids* **2010**:710589. DOI: <https://doi.org/10.4061/2010/710589>, PMID: 20847952
- Thomas A, Bates S, Figg WD, Pommier Y. 2017. DNA topoisomerase targeting drugs. In: Bast R. C, Croce C. M, Hait W. N, Hong W. K, Kufe D, Piccard-Gebhart M, Pollock R. E, Weichselbaum R. R, Wang H, Holland J. F (Eds). *Holland-Frei Cancer Medicine*. Hoboken, NJ: John Wiley & Sons, Inc. p. 665–678.
- von Metzler I, Heider U, Mieth M, Lamottke B, Kaiser M, Jakob C, Sezer O. 2009. Synergistic interaction of proteasome and topoisomerase II inhibition in multiple myeloma. *Experimental Cell Research* **315**:2471–2478. DOI: <https://doi.org/10.1016/j.yexcr.2009.04.019>, PMID: 19410573

- Willmore E**, Frank AJ, Padgett K, Tilby MJ, Austin CA. 1998. Etoposide targets topoisomerase IIalpha and IIbeta in leukemic cells: isoform-specific cleavable complexes visualized and *quantified* in situ by a novel immunofluorescence technique. *Molecular Pharmacology* **54**:78–85. DOI: <https://doi.org/10.1124/mol.54.1.78>, PMID: 9658192
- Zagnoli-Vieiral G**, Caldecott KW. 2017. Tdp2, top2 And SUMO: What Is ZATT About? *Cell Research* **27**:1405–1406. DOI: <https://doi.org/10.1038/cr.2017.147>
- Zhang A**, Lyu YL, Lin CP, Zhou N, Azarova AM, Wood LM, Liu LF. 2006. A protease pathway for the repair of topoisomerase II-DNA covalent complexes. *Journal of Biological Chemistry* **281**:35997–36003. DOI: <https://doi.org/10.1074/jbc.M604149200>, PMID: 16973621
- Zhang Y**, Liu T, Meyer CA, Eeckhoute J, Johnson DS, Bernstein BE, Nusbaum C, Myers RM, Brown M, Li W, Liu XS. 2008. Model-based analysis of ChIP-Seq (MACS). *Genome Biology* **9**:R137. DOI: <https://doi.org/10.1186/gb-2008-9-9-r137>, PMID: 18798982
- Zhang CZ**, Leibowitz ML, Pellman D. 2013. Chromothripsis and beyond: rapid genome evolution from complex chromosomal rearrangements. *Genes & Development* **27**:2513–2530. DOI: <https://doi.org/10.1101/gad.229559.113>, PMID: 24298051
- Zong D**, Adam S, Wang Y, Sasanuma H, Callén E, Murga M, Day A, Kruhlak MJ, Wong N, Munro M, Ray Chaudhuri A, Karim B, Xia B, Takeda S, Johnson N, Durocher D, Nussenzweig A. 2019. BRCA1 haploinsufficiency is masked by RNF168-Mediated chromatin ubiquitylation. *Molecular Cell* **73**:1267–1281. DOI: <https://doi.org/10.1016/j.molcel.2018.12.010>, PMID: 30704900